



HAL
open science

Tectonic and climate control on allochthonous bauxite deposition. Example from the mid-Cretaceous Villeveyrac basin, southern France

Emmanuelle Chanvry, Emilie Marchand, Michel Lopez, Michel Séranne,
Gwenn Le Saout, Marc Vinches

► To cite this version:

Emmanuelle Chanvry, Emilie Marchand, Michel Lopez, Michel Séranne, Gwenn Le Saout, et al.. Tectonic and climate control on allochthonous bauxite deposition. Example from the mid-Cretaceous Villeveyrac basin, southern France. *Sedimentary Geology*, 2020, 407, pp.105727. 10.1016/j.sedgeo.2020.105727 . hal-02913633

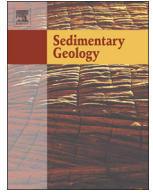
HAL Id: hal-02913633

<https://imt-mines-ales.hal.science/hal-02913633>

Submitted on 13 Nov 2020

HAL is a multi-disciplinary open access archive for the deposit and dissemination of scientific research documents, whether they are published or not. The documents may come from teaching and research institutions in France or abroad, or from public or private research centers.

L'archive ouverte pluridisciplinaire **HAL**, est destinée au dépôt et à la diffusion de documents scientifiques de niveau recherche, publiés ou non, émanant des établissements d'enseignement et de recherche français ou étrangers, des laboratoires publics ou privés.



Tectonic and climate control on allochthonous bauxite deposition. Example from the mid-Cretaceous Villeveyrac basin, southern France

Emmanuelle Chanvry^{a,*}, Emilie Marchand^{a,b}, Michel Lopez^a, Michel Séranne^a, Gwenn Le Saout^c, Marc Vinches^b

^a Géosciences Montpellier, Université de Montpellier, CNRS, 34095 Montpellier cedex 05, France

^b GEI, IMT Mines Alès, 6 avenue de Clavières, 30319 Alès Cedex, France

^c LMGC, IMT Mines Ales, Univ Montpellier, CNRS, 6 avenue de Clavières, 30319 Alès Cedex, France

ARTICLE INFO

Article history:

Received 30 April 2020

Received in revised form 15 July 2020

Accepted 16 July 2020

Available online 22 July 2020

Editor: Dr. Jasper Knight

Keywords:

Karstic bauxite

Pedofacies

Debris-flow

Paralic environment

Clay minerals

Albian climate

ABSTRACT

Karst bauxite deposits represent 11% of the global quantity of bauxite (Bardossy and Aleva, 1990). Karst Bauxite is defined as bauxite deposits overlying carbonate rocks above a more or less karstified surface. Allochthonous karst bauxites result from two successive processes: (1) intense weathering and formation of a lateritic profile, involving the development of bauxitic and duricrust horizons; and (2) erosion of the lateritic profile and deposition above a carbonate unit located downstream. In the Villeveyrac basin (southern France), Lower to Mid-Albian allochthonous karstic bauxites are deposited on a Jurassic karstified bedrock, and are overlain by a Late Albian marine siliciclastic cover. A drillcore, sampling the substratum, the bauxites and their cover, is analyzed and offers the opportunity to investigate the depositional conditions and interactions of climate and tectonic during the mid- to late Cretaceous, through the analysis of mechanical and chemical weathering evidence. Sedimentological study allowed the definition of four bauxite facies and three siliciclastic cover facies, overprinted by four different pedofacies. Mineralogical and geochemical analyses allowed the distinction of four mineralogical units controlled by climate-related weathering processes. The bauxite deposits emplaced by mud-flow/debris-flow gravity currents are composed by boehmite-hematite and goethite. The top of the bauxite presents a progressive upward decrease in Al_2O_3 and TiO_2 associated with the occurrence of kaolinite. The base of the cover that overlies the bauxite interval corresponds to a paralic environment, dominated by kaolinite, with a sub-ferricrete paleosol. The following paralic sequence presents a clay-rich suite dominated by smectite, associated with mica/illite and quartz, which suggests aridification of climate around the latest Albian. We interpret this sedimentary succession as the result of erosion of an autochthonous laterite cover, induced by major tectonic uplift in the upstream drainage area, which led to a significant increase in slope gradient, under a wet tropical climate. Mechanical erosion of autochthonous laterite bauxite in the upstream drainage led to a reverse stacking of the reworked autochthonous lateritic profile in the depositional basin. A continuous transgressive trend was responsible for trapping of the allochthonous karst bauxite. This was followed by stacking of siliciclastic paralic sequences, which record progressive erosion of the bedrock in the upstream drainage area, under dry tropical conditions. Our results thus suggest that dismantling of the autochthonous laterite cover was initiated by Albian uplift and this ended with a change towards drier and more seasonal climate at the Albian-Cenomanian transition.

© 2020 Elsevier B.V. All rights reserved.

1. Introduction

Since Erhart (1956) theorized the bio-rhexistasy concept, paleosols represent an efficient tool to identify climate changes within continental sedimentary successions: they link the phytogeography of the landscape with climate-controlled weathering conditions. In particular, the initial fabric and mineralogy of pedologic profiles are clearly climatic-

dependent and mostly reflect the temperature, humidity, evapotranspiration, hydrogeochemistry and drainage conditions of the exposed surfaces (Erhart, 1966; Frakes, 1979; Parrish, 1998). The main challenge is to discriminate the respective parts of diagenetic and epigenetic transformations in order to characterize the initial regolith (Nesbitt, 1992; Wright, 1992; Sheldon and Tabor, 2009). In particular, H^+ activity is directly linked to the weathering characteristics of the paleosol (Kämpf and Schwertmann, 1983; Lukens et al., 2018). This pedogenetic approach has been used to discriminate humid tropical and subtropical climate conditions which control the formation of ferrallitic paleosols, such as bauxites, when tectonics, hydrogeology and lithology of the

* Corresponding author at: Emmanuelle Chanvry, Géosciences Montpellier, Université de Montpellier, Case 060, 34095 Montpellier Cedex 5, France.

E-mail address: emmanuelle.chanvry@hotmail.fr (E. Chanvry).

source rock are favorable (Bardossy, 1982; Bardossy and Aleva, 1990; Föllmi et al., 1993; D'Argenio and Mindszenty, 1995). Bauxite represents a particular laterite type, which results from intense continental weathering, and is composed of alumina (no less than 45–50% Al_2O_3) and ferric iron hydrates (no more than 20% Fe_2O_3), titanium oxide, and combined silica and clay minerals (mainly kaolinite) (Valeton, 1972). Bauxite represents a mature laterite submitted to intense vertical leaching, where alkalis, alkaline earths and silica are removed.

Cretaceous bauxite deposits of the Tethyan realm represent a particularly relevant example of long-lasting greenhouse conditions in sub-aerially exposed areas (Bardossy and Aleva, 1990; Retallack, 2010). The high peak of bauxite formation during the mid-Cretaceous was related to: (i) the high oxygen content of the atmosphere during this period (Budyko et al., 1987; Combes and Bardossy, 1994), and (ii) a globally warm and wet climate (Frakes, 1979; Garrels, 1983; Arthur et al., 1985; Larson, 1991), with an extension of the monsoon belt over large continental areas (Bardossy and Aleva, 1990). More recently, Mindszenty (2016) suggested that bauxite development might have acted as one of the feedback processes leading the cessation of Cretaceous greenhouse conditions by slowing down oxidative weathering on land.

The karst bauxite deposits of the Northern Tethyan realm developed on carbonate platforms of tectonically mobile belts (Bardossy and Combes, 1999) during the mid-Cretaceous peak of bauxitization. The allochthonous (clastic) to parautochthonous (mixed clastic and in situ) bauxite deposits were trapped into funnel-shaped sinkholes displaying complex infilling, which records both base-level variations and repeated inputs from the surrounding dismantled autochthonous lateritic profiles (Combes, 1969, 1973, 1984). Only the “Ariège-type deposits” in southern France show a gradual transition from shallow marine claystones and marls to mostly pisolitic bauxite, interpreted as the result of an autochthonous bauxitization process, during sea-level lowstands (Combes, 1990; Bardossy and Combes, 1999).

Thus, the study of a whole section, from allochthonous karst bauxite up to the sedimentary cover, can help characterize the conditions of bauxitization, dismantling, and finally the disappearance of bauxite in the sedimentary succession, in order to evaluate the respective roles played by climate and tectonics. The Villeveyrac basin in southern France provides outcrops, mine-works and drillcores, made available by SODICAPEI mining company. We investigate a representative drillcore, selected after a complete regional study, based on the analyses of outcrops and a substantial drill-hole data base (Marchand, 2019). We present a detailed facies analysis, including *syn*- and postdepositional processes, strengthened by petrographical analysis, in order to define depositional environments for the bauxite and its sedimentary cover. This approach is supported by bulk and clay mineralogy analyses, through the complete sedimentary succession, coupled to the evolution of the geochemical record. We then discuss the impact of climate versus tectonics in the occurrence, evolution and disappearance of bauxite.

2. Geological setting of the Villeveyrac basin

The Villeveyrac basin is located between the Variscan basement structural high (Massif Central) and the present-day Mediterranean Sea, on the uplifted ‘Isthme Durancien’ domain (Gignoux, 1926) (Fig. 1). This area was previously affected by Tethysian rifting leading to the development of a wide carbonate platform from the Liassic to the early Cretaceous (Hauterivian), onlapping the crystalline and metasedimentary Variscan basement to the northwest (Dubois and Delfaud, 1989). This marine sedimentary succession was interrupted during the Neocomian, when the opening of the North Atlantic Ocean induced differential movement between the SW margin of the Eurasian plate with Iberia and associated small continental blocks. This period was characterized by the development of a highly subsident E-W trending elongated Pyrenean rift (e.g., Lagabrielle et al., 2010), extending eastwards to southern Provence (Fournier et al., 2016). This area is

now filled with deep marine sediments (e.g., Debroas, 1990) bordered by uplifted margins (Wyns et al., 2003). In the Languedoc-Provence area, the onshore uplifted domain, known as the ‘Isthme Durancien’ (Gignoux, 1926), underwent long subaerial exposure on the sedimentary and crystalline basement and the Neocomian marls (Fig. 1B), with intense erosion and denudation (Barbarand et al., 2001; Séranne et al., 2002). Between the Aptian and Albian, wet tropical conditions led to the development of bauxite deposits recording a major hiatus in the sedimentary depositional cycle (Bardossy and Combes, 1999; Alabouvette et al., 2003). In the Villeveyrac basin, allochthonous bauxite deposition corresponds to the shortest time interval from the Lower to Mid Albian (Demangeon, 1965; Combes, 1969, 1990; Marchand et al., 2020). This allochthonous karst bauxite interval is covered by a transgressive shallow marine siliciclastic sequence, reported to the latest Albian (“Vraconien”; Husson, 2013). During the late Cretaceous, sediments evolved towards a continental and regressively siliciclastic sequence, which records the initiation of Pyrenean compression.

3. Data and methods

The present study is based on analysis of the 13-OL-184 drillcore provided by the SODICAPEI Company, which mines bauxite in the Villeveyrac basin (Fig. 1A). The 190 m long drillcore, logged at 1/200 scale, displays a complete section from the karstified Jurassic basement, overlain by 6 m of bauxite, and covered by the siliciclastic late Cretaceous cover (Fig. 2). The average bauxite thickness found in this basin is 4 m (Marchand, 2019), which makes the drillcore a significant sample of the bauxite interval. Furthermore, the drillcore exhibits a recovery rate of about 97%, and thus provides a good representative section of the sedimentary succession of the basin (Marchand, 2019).

Facies analyses included characterization of the lithology, texture, bedding pattern, sedimentary structures, bioturbations and organic and non-organic contents, with the aim to define facies, depositional processes, and paleoenvironments. To better constrain the depositional processes, we selected three samples from the bauxite interval and ten very fine to fine grained samples in the siliciclastic late Cretaceous cover for microscopic study under reflected and transmitted light (Fig. 2). The selection was made considering the facies type, and the homogeneity of the sedimentary succession. From this, special attention was paid to the base of the siliciclastic cover (six samples) showing high facies variability.

The bauxite and siliciclastic cover mineralogy was firstly characterized using X Ray Powder Diffraction (XRD). Three samples were analyzed in the bauxite interval, and seven in the siliciclastic interval. XRD analyses were performed on a diffractometer BRUKER D8 Advance using a Lynxeye detector. Standard powder diffractograms were acquired with 120-min duration on a 2θ range of 1.4° to 20° ($\text{Cu K}\alpha$, 1.54 \AA). Bulk XRD results were analyzed using XPower software to provide semi-quantitative measurements of mineral compositions. The samples showing a significant quantity of clay where the clay diffraction peak are recognized were then studied considering the fraction below $2 \mu\text{m}$ to identify the clay mineralogical associations, in order to discuss weathering conditions throughout the sedimentary profile. Clay mineral analyses were carried out on oriented mounts of representative samples from each facies. Typically, for XRD mineral analysis, the clay fractions ($<2 \mu\text{m}$) of argillaceous rock samples were separated by means of gentle crushing and ultrasonic disintegration, followed by grain size separation by means of centrifugation or settling (Larqué and Weber, 1975). The identification of clay minerals was made according to the position of the (001) series of basal reflections on the diffractogram (Brindley and Brown, 1980). Air-dried (natural) preparations were analyzed from all samples and, where needed, ethylene-glycol treatment was used to distinguish overlapping XRD-peaks and expandable clay minerals (Hardy and Tucker, 1984). Graphical comparisons between XRD-peaks (for example the 7A d001 peak of kaolinite and 16A d001 peak of smectite) were used to estimate the

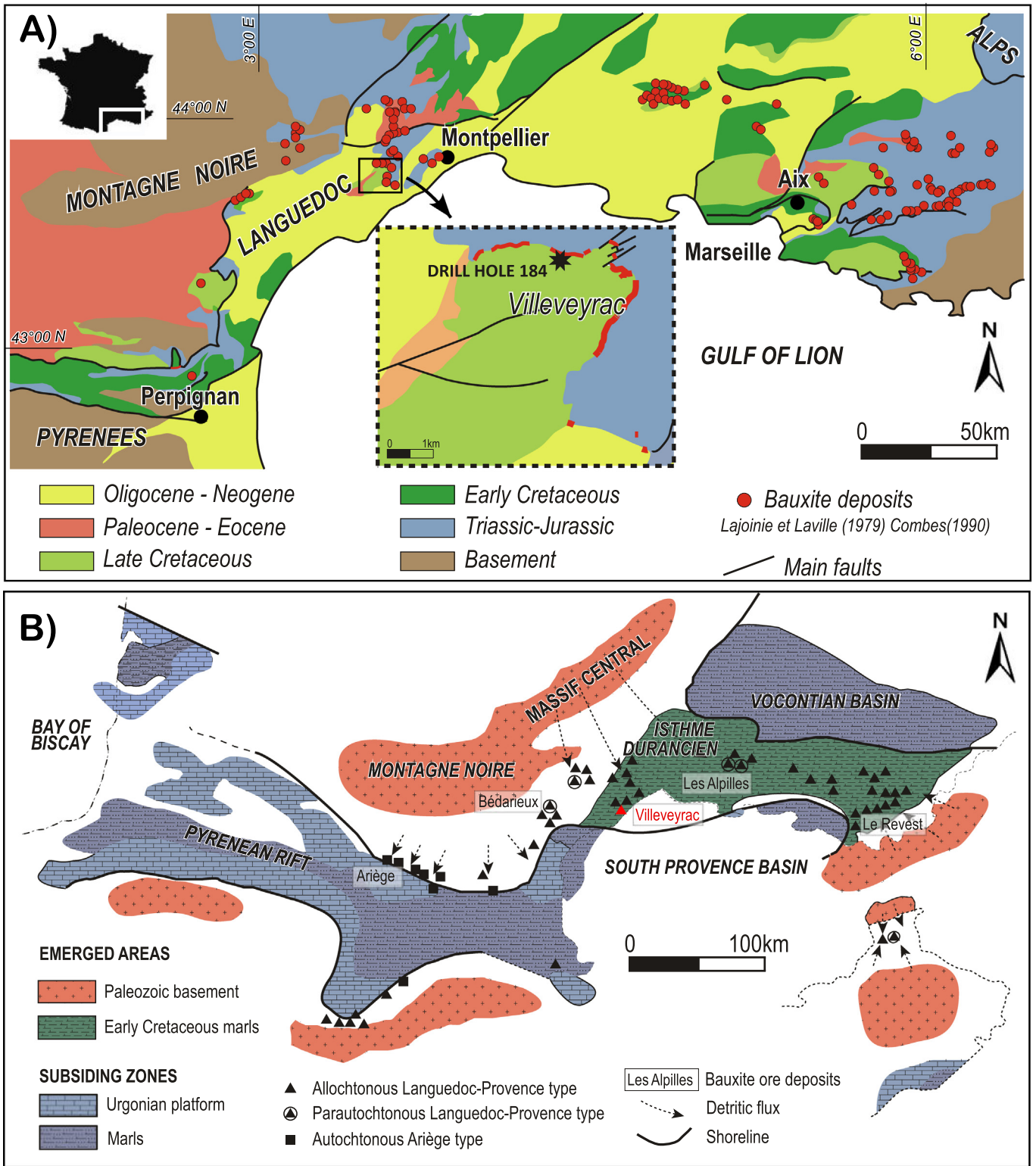


Fig. 1. Geological and paleogeographical context of the Pyrénéo-Provençal bauxites. (A) Geological map of the South of France with distribution of the bauxite ore deposits (red dots). The dotted square and enlarged detailed map corresponds to the Villeveyrac basin. (B) Paleogeographic map of the European and Iberian margins during Mid-Cretaceous showing the distribution of the different types of bauxite, dominantly allocthonous or parautocthonous. From Marchand (2019), modified after Araud-Vanneau et al. (1979) and Combes (1990). (For interpretation of the references to color in this figure legend, the reader is referred to the web version of this article.)

appearance and relative increase or decrease of each phase within the individual sedimentary successions.

Based on XRD results, the geochemistry of the transition between bauxite interval and siliciclastic cover showing the main mineral

changes was studied with a portable X-Ray fluorescence spectrometer (NITON XL3t 900 Analyzer). Major elements were obtained using the Mining Mode and are converted in oxide %wt. The accuracy of the analyses is around 5% for the major elements. The analyses were done from

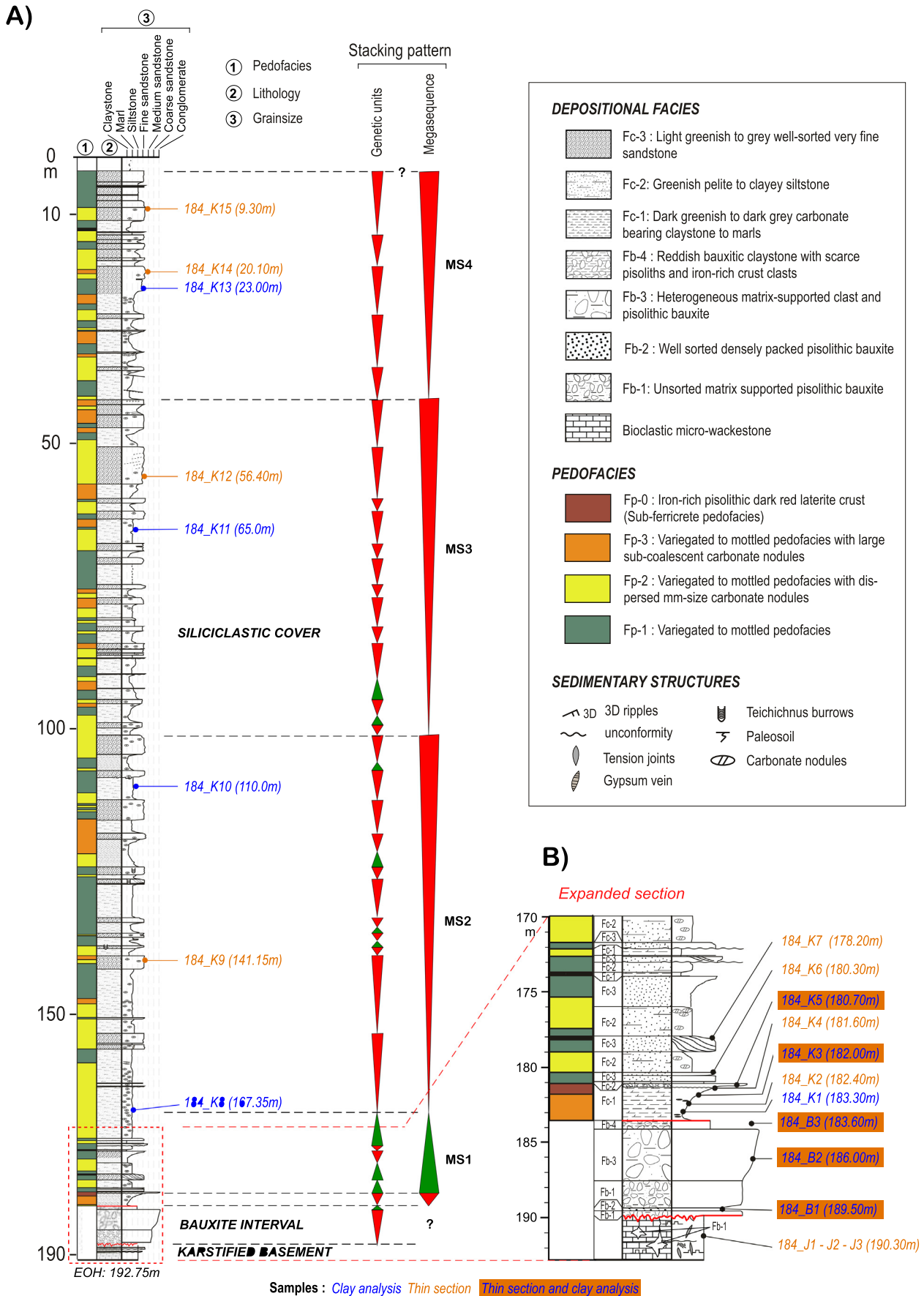


Fig. 2. Sedimentological descriptions of the core 13-OL-184. (A) Complete core section showing: (1) color-coded pedofacies, (2) lithofacies and (3) grain size and stacking pattern on the right. Sample position is indicated as well as analytical methods used. (B) High resolution, detailed log of the bauxite interval.

189 to 176 m depth with a sampling step ranging from 10 to 40 cm, depending on facies variability ($n = 80$ in total). Only data with a relative error less than 5% were selected ($n = 39$).

4. Results

Coupled high-resolution sedimentological, mineralogical and geochemical studies of the drillcore 13-OL-184 allow us to distinguish, above the Upper Jurassic karstified basement, a bauxite interval separated by a major paleosol from a cover interval (Fig. 2). The facies analysis gives evidence for seven lithofacies in the bauxite interval and the siliciclastic cover. These facies correspond to major depositional processes and constrain the paleoenvironment evolution of the zone. In addition, four post-depositional facies related to material redistribution during pedogenesis and water-table fluctuations were identified, which constrain climate and base-level changes.

4.1. Facies analysis and depositional processes

4.1.1. The Upper Jurassic karstified basement

The footwall of the bauxite deposits is represented by about 3 m at the base of the drillcore (Fig. 2). These deposits are mainly composed of grey homogeneous bioclastic microwackestone, including lamellibranch and echinoid debris, related to Upper Jurassic outer platform deposits (Fig. 3A–C). These facies locally show abundant stylolites thinly stained by dark red silty clay stringers and associated with cm-sized wine-red

mottling (Fig. 3B). These structures are crossed by oblique to sub-perpendicular veins walled by early syntaxial subhedral sparite and partly filled both by reddish calcite blocky cement and late dark-red silty claystone (Fig. 3D). Some of these veins are partly enlarged and interconnected to cm- to dm-size star-like karstic cavities filled by massive brown-red fine-grained bauxite (Fig. 3A). The silt to sand fraction (Fig. 3B, D) is represented by dark red iron-rich debris including quartz, calcite and subhedral dolomite fragments consistent with the downward percolation of bauxitic vadose silt into the early fracture and endokarst network.

4.1.2. Bauxite interval facies analysis

The bauxite ore deposit is about 6.5 m thick. The bauxite in the drillcore is affected by intense fracturing and splits along thin bedding, resulting in a crumbly texture. Four main lithofacies are distinguished depending on the abundance and size of the clastic fraction including pisolithic laterite, iron-rich crust debris and pisoliths (Fig. 4). The contact between the different lithofacies is subtle and often transitional. The bauxite interval displays several color changes from white, brown red, pinkish-red to orange, which are related to post-depositional processes (Marchand, 2019). For this reason, color has not been taken into account for the primary facies characterization of the bauxite ore deposit.

4.1.2.1. Unsorted matrix supported pisolithic bauxite (Facies Fb-1). This facies is common throughout the bauxite interval (2 m total thickness). It is characterized by hematite-rich pisoliths ranging from 200 μm to more

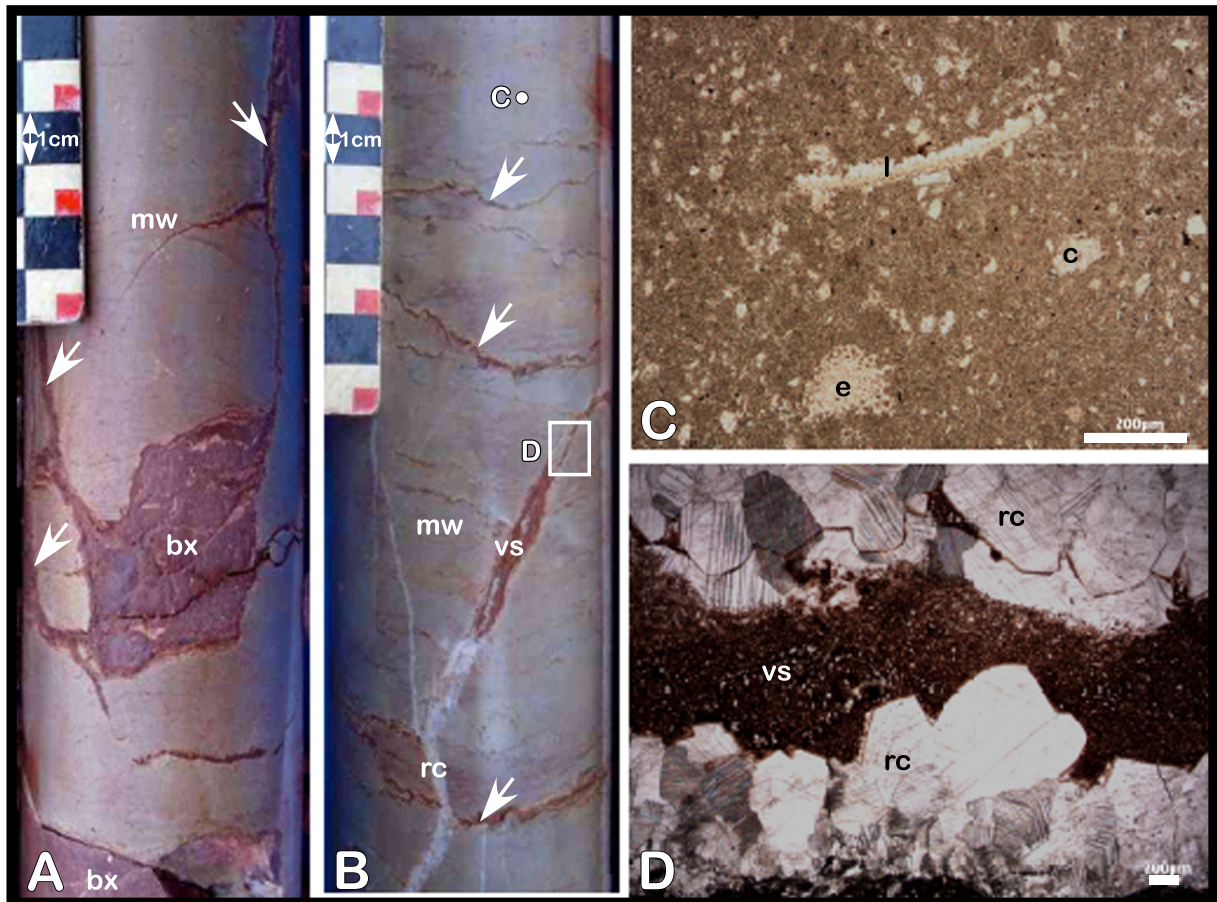


Fig. 3. Facies and microfacies characterization of the Upper Jurassic karstified basement. (A) Slightly variegated microwackestone (mw) crossed by a bauxite-filled star-like endokarst (bx). The cavities are interconnected by a dense fracture network (white arrows). (B) Variegated microwackestone (mw) showing irregular stylolites (white arrows) stained by red vadose siltstone, and intersected by radiaxial calcite veins (rc). Some veins are partly reopened and filled with red vadose siltstone (vs). (C) Thin section of the microwackestone showing dispersed echinoderms (e), lamellibranch (l) and calcite debris (c) floating into a muddy fabric (Plane-Polarized Light [PPL]). (D) Thin section of a radiaxial calcite vein (rc) partly filled with brown vadose siltstone (vs) in the axial zone (PPL), see (B) for location. (For interpretation of the references to color in this figure legend, the reader is referred to the web version of this article.)

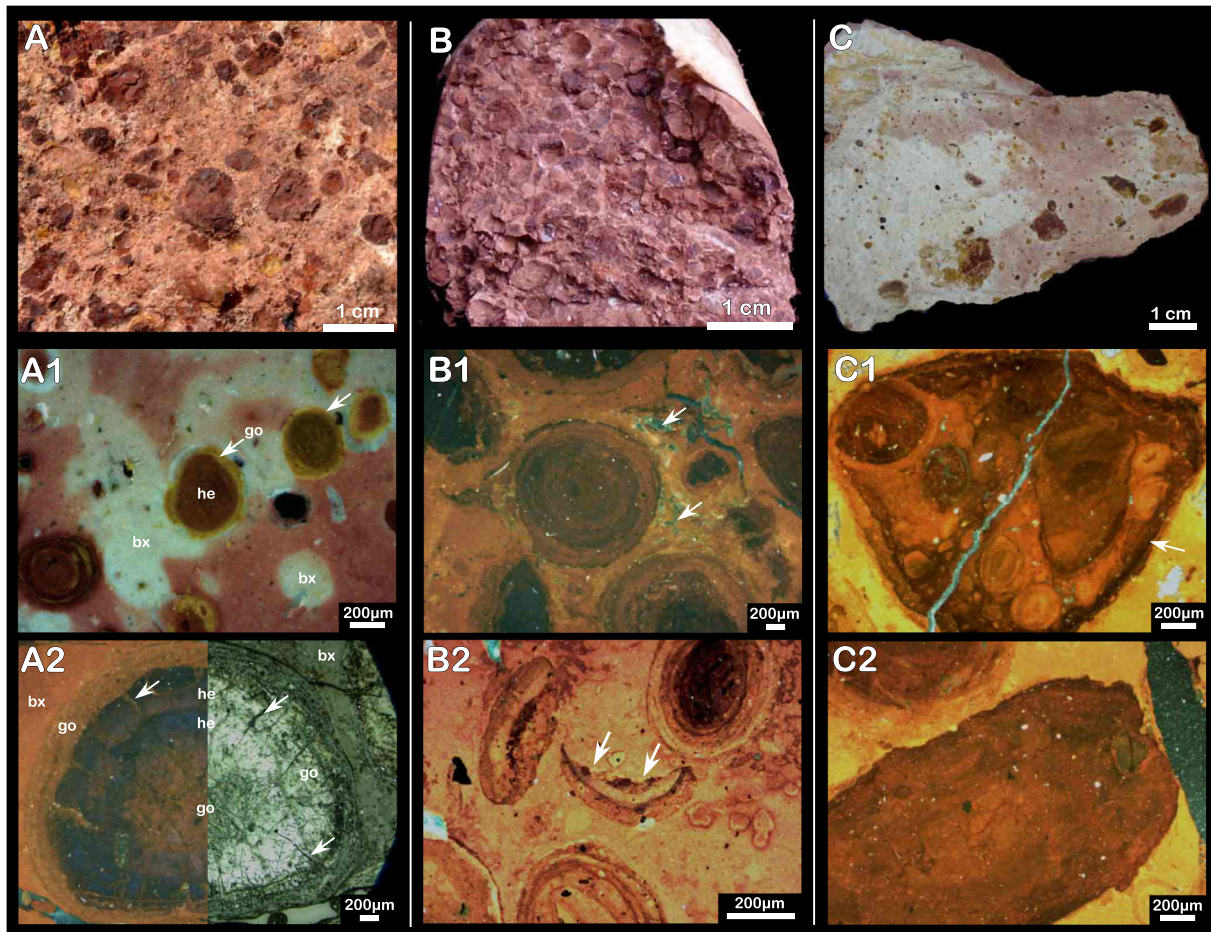


Fig. 4. Macro- and microfacies characterization of the bauxite interval. (A) Unsorted matrix supported pisolithic bauxite (Fb-1). (A1) Thin-section showing dispersed pisoliths of variable composition, from hematite-rich (he) with often a goethite coating (go) to boehmite-rich (bx) into a red to white aluminous-rich matrix (Cross-Polarized reflected Light [CPRL]). (A2) Detailed view of a pisolith showing successive goethite-rich (go) and hematite-rich (he) envelopes floating into an iron and aluminous-rich matrix (bx) Left: CPRL; Right: Plane Polarize Reflected Light [PPRL]. (B) Well sorted densely packed pisolithic bauxite (Fb-2). (B1) Thin-section showing clast-supported hematite-rich regular pisoliths packed into a lighter aluminous-rich matrix with residual intergranular porosity (white arrow, CPRL). (B2) Thin-section showing densely packed pisolithic bauxite including broken grains (white arrows, CPRL). (C) Heterogeneous matrix-supported clast and pisolith bauxite (Fb-3). (C1) Thin-section, showing pisolithic bauxite fragment (CPRL). (C2) Thin-section showing a clast of hematite crust (CPRL). (For interpretation of the references to color in this figure legend, the reader is referred to the web version of this article.)

than 1 cm, floating in silt sized homogeneous iron and aluminous-rich matrix. The pisoliths and iron-rich clast are partly broken with cutaways and locally angular limits indicating some mechanical reworking (Fig. 4B2). Some pisoliths show a light-colored coating (Fig. 4A). In thin section, different types of pisoliths and grains are identified including iron-rich matrix with residual intergranular porosity (white arrow, CPRL). Most of these pisoliths show a goethitic coating (Fig. 4A1). The matrix of the bauxitic material ranges from red (Fig. 4A, B) to white (Fig. 4C) with possible intermediate facies showing irregular patches (Fig. 4A1). We interpreted the white matrix as iron free aluminium hydroxides enriched by Fe leaching as proposed by Boulange et al. (1997) with the pisolithic nodules mainly composed of goethite and possible hematite (Nahon, 1986) with up to 25% mol of AlOOH (Boulange et al., 1997). Numerous pisoliths show successive cortical envelopes varying in color from dark red-brown to yellowish-orange both on hand samples under direct natural light and in thin section under cross-polarized reflected light (Fig. 4A1, B1, C1, B2). These color variations were clearly linked to a change in main mineral composition from goethite-rich (yellowish) to hematite-rich (reddish brown) supported by XRD analysis and Mossbauer spectroscopy by Scheinost and Schwertmann (1999), and confirmed in numerous iron nodules of ferric soils by coupled thin section analysis and Raman spectroscopy (Ramanidou, 2009;

Löhr et al., 2013). Moreover plane-polarized reflected light (Fig. 4A2) confirms the main mineral composition of the pisoliths with a light bluish grey color for hematite and a medium to dark grey color for goethite (Spry and Gedlinske, 1987; Pracejus, 2008). These mineral composition variations suggest periodic changes in chemical conditions in the initial autochthonous bauxite deposit. The presence of radial v-shaped cracks (Fig. 4A2) suggests early contraction before the last goethite coating, as is discussed by Anand and Verrall (2011).

The Fb-1 facies is interpreted as the reworking and limited mass-transportation of an unconsolidated matrix-rich bauxitic material, compatible with a mudflow-dominated process involving both steep slope and heavy rain to trigger a gravitational current (Valeton, 1972; Valeton et al., 1987; Combes and Bardossy, 1995; D'Argenio and Mindszenty, 1995).

4.1.2.2. Well-sorted densely packed pisolithic bauxite (Facies Fb-2). This facies forms a 15 cm-thick layer close to the base of the bauxite interval with a sharp base and top. It is mainly composed of mm- to cm-scale well-sorted iron-rich pisoliths, showing a close grain-supported fabric (Fig. 4B). Most pisoliths display a peripheral light-colored coating. The intergranular space is partly filled by muddy matrix with local residual porosity and voids (Fig. 4B1). The regular laminar coating around the

nucleus is well expressed in the pisoliths (Fig. B1). Some pisoliths are broken, indicating reworking under high energy conditions (Fig. 4B2).

The Fb-2 facies is consistent with bedload transport under a high energy diluted current during the end of a flood event (Valeton, 1972; Mindszenty, 2010).

4.1.2.3. Heterogeneous matrix-supported clast and pisolith bauxite (Facies Fb-3). The heterogeneous matrix-supported bauxite (Fig. 4C) is the most common facies of thbauxite interval, representing a cumulative thickness of about 4.5 m. It includes clasts of both iron-rich crust (Fig. 4C2) and pisolithic early (primary?) bauxite varying in size from a few millimeters to several centimeters, which float in a muddy matrix, including dispersed iron-rich pisoliths (Fig. 4C1). The matrix and the clasts contain a silt-sized quartz fraction (Fig. 4C2). The size and abundance of the clastic fraction varies randomly through the bauxite section and is not associated with any bedding fabric.

The Fb-3 facies is interpreted as reworking of partly consolidated autochthonous lateritic bauxite clasts transported as a debrisflow. As for Facies Fb-1, this implies slope instability. In this case, the abundance of iron-crust debris relative to pisolithic bauxite clasts suggests reworking of the hardened uppermost part of the autochthonous lateritic profile

(Valeton, 1972; Valeton et al., 1987; Combes and Bardossy, 1995; D'Argenio and Mindszenty, 1995).

4.1.2.4. Reddish bauxitic claystone with scarce pisoliths and iron-rich crust clasts (Facies Fb-4). This facies develops is 50 cm thick at the top of the bauxite interval and shows fine-grained deposit including dispersed pisoliths or iron-crust debris (Fig. 5A). The muddy fraction contains abundant white glossy clayey halos (probably kaolinite) and an irregular orange staining associated with the presence of goethite (Fig. 5B).

The Fb-4 facies records mudflow deposition at the top of the bauxite sequence, in agreement with the paucity of the consolidated autochthonous lateritic material in the source area (Mindszenty, 2010). The significance of the clayey fraction will be discussed in the light of the mineralogy and geochemistry.

4.1.3. The siliciclastic cover facies analyses

The 181 m-long recovered siliciclastic cover is mainly composed of a repetitive greenish grey succession of claystone to fine sandstone deposits, slightly to intensely affected by dark red to orange pedogenic mottling. The pedogenic overprint is considered as a post-depositional process and will be described separately (Section 4.1.2.3). Three lithofacies are recognized in this interval (Fig. 6).

4.1.3.1. Dark greenish to dark grey carbonate bearing claystone to marls (Facies Fc-1). This facies is a muddy facies, which is particularly crumbly (Fig. 6A). It displays a transitional base and top. It is moderately to highly stained by pedogenesis or crossed by a thin rootlet network (Fig. 6A1). The carbonate content is variable, ranging from carbonate barren (i.e., pure claystone) to carbonate claystone or even marls. The silt-size fraction is low to absent. In thin-section, this facies appears relatively homogeneous with dispersed black organic speckles (Fig. 6A2).

Fc-1 facies is interpreted as suspension settling in a quiet, shallow-water environment periodically affected by subaerial exposure (Reynolds, 1996).

4.1.3.2. Greenish pelite to clayey siltstone (Facies Fc-2). This facies corresponds to a continuous series with a transitional base and top ranging from silty claystones (i.e., pelites) to clayey siltstones. In thin section, the silt-size quartz fraction appears homogeneous, ranging in size from 10 to 80 μm , and includes dispersed very fine sand grains and rare pellets (Fig. 6B1). The greenish depositional color is generally overprinted by a sustained mottling, evidenced by dark red to orange staining (Fig. 6B). This facies presents pedogenetic white carbonate nodule clusters (see Section 4.1.2.3).

Fc-2 facies marks suspension settling with periodic distal terrestrial input into a very protected marine domain (Reynolds, 1996; Diessel, 2012).

4.1.3.3. Light greenish to grey well-sorted very fine sandstone (Facies Fc-3). Fc-3 facies is characterized by homogeneous, massive, sharp-based very fine sandstone, intensely bioturbated by *Teichichnus* burrows underlined by orange iron oxides (Fig. 6C, C2, C3). 3D ascending current ripples have been observed in the lower part of the series. In thin section, the sand fraction is well sorted and dominated by angular to sub-angular quartz grains, rare feldspars, micas and dispersed, partly dissociated, dark pellets. The clastic fraction is bounded by a carbonate rich matrix (Fig. 6C1, C4). Towards the top of the drillcore, Fc-3 facies contains rare dispersed glauconite grains (Fig. 6C4).

The Fc-3 facies is interpreted as periodic fine-grained detrital supply under moderate tractive currents and associated decantation into a very low energy nutrient-rich shallow water domain affected by intense burrowing.

4.1.4. Pedofacies analysis

In contrast with the bauxite interval, the siliciclastic cover is intensely overprinted by early pedogenesis. This reflects the conditions

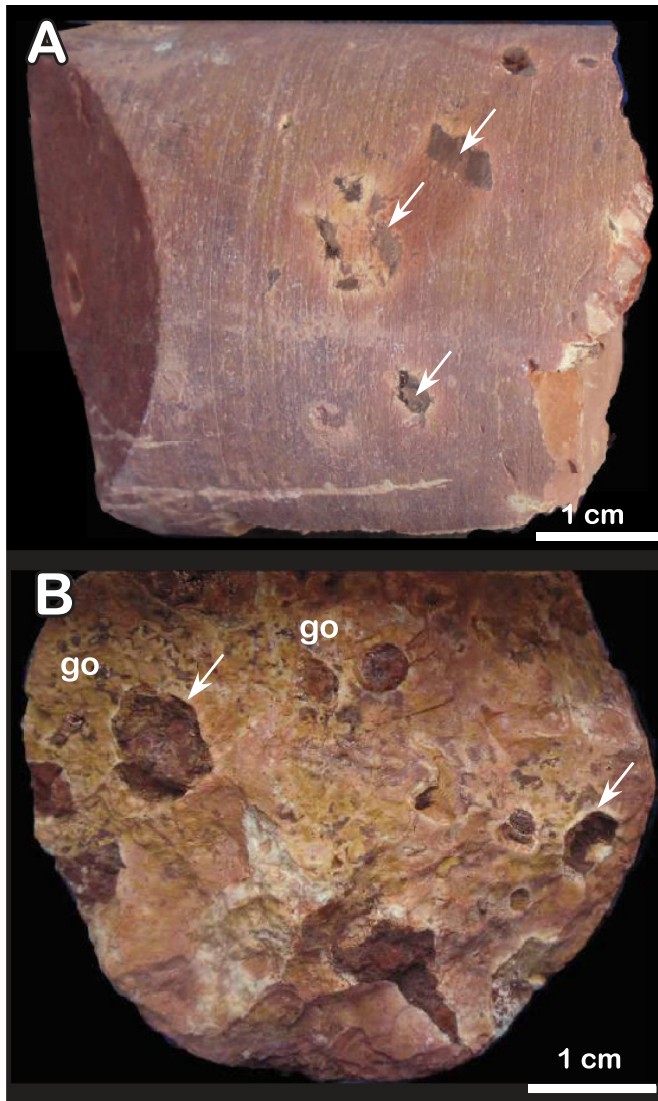


Fig. 5. Close-up view of the reddish bauxitic claystone (Fb-4) at the top of the bauxite interval, as seen on the cores. (A) Massive muddy facies with scarce iron-crust debris (white arrows). (B) Alternative facies including dispersed iron-crust and pisoliths debris; white arrows: white glossy halo; go: goethite plating.

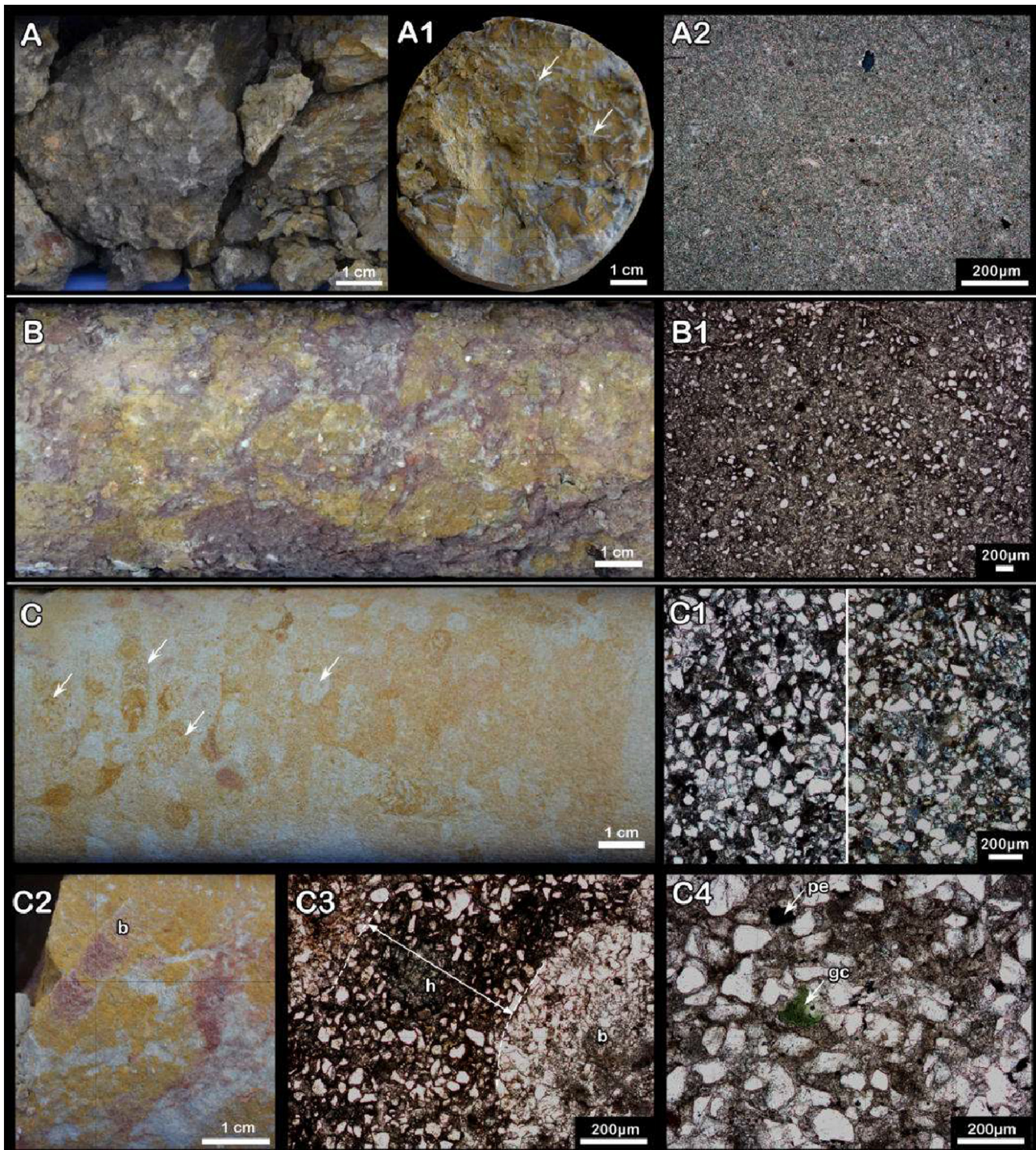


Fig. 6. Macro- and microfacies characterization of the siliciclastic cover. (A) Dark greenish carbonate bearing claystone as seen on fragmented core. (Fc-1). (A1) Core section showing slight variegated marl stained by iron oxides and crossed by rootlets (white arrows). (A2) Thin-section showing a homogeneous clayey carbonate bearing microfabric (Cross-Polarized Light). (B) Greenish pelite to clayey siltstone (Fc-2). (B1) Thin-section showing a homogeneous dispersed silt-size quartz fraction into the clayey, carbonate bearing, matrix (Plane-Polarized Light, PPL). (C) light-Greenish well-sorted very fine sandstone (Fc-3); white arrows: *Teichichnus* burrow. (C1) Thin-section showing relatively well sorted very fine sand-size Fc-3 facies (left PPL and right CPL). (C2) Core showing a *Teichichnus* burrow (b). (C3) Thin-section perpendicular to a *Teichichnus* burrow showing the very fine quartz sand dense packing into the burrow conduit (b) surrounded by a dark iron-rich halo (h) produce by oxidation of the walls during animal activity (PPL). (C4) Very fine sand bounded by a carbonate-rich matrix composed dominantly by angular to subangular quartz grains with dispersed, partly dissociated pellets (pe) and glauconite (gc) grains (PPL).

of subaerial exposure. In particular it provides information on duration of exposure, water table position, depth of vertical leaching, phytogeography and climate (Erhart, 1966; Frakes, 1979; Parrish, 1998). Four main pedogenetic facies are distinguished. Where present, these are associated with depositional facies in the sedimentological description.

4.1.4.1. Iron-rich pisolithic dark red laterite crust sub-ferricrete pedofacies (Fp-0). This facies was only identified in the first sequence capping the bauxite interval (Fig. 7). It is characterized by a dominant dark red to orange, indurated material, including dispersed pisoliths with an upward increase in coarsening and packing. Pisoliths have

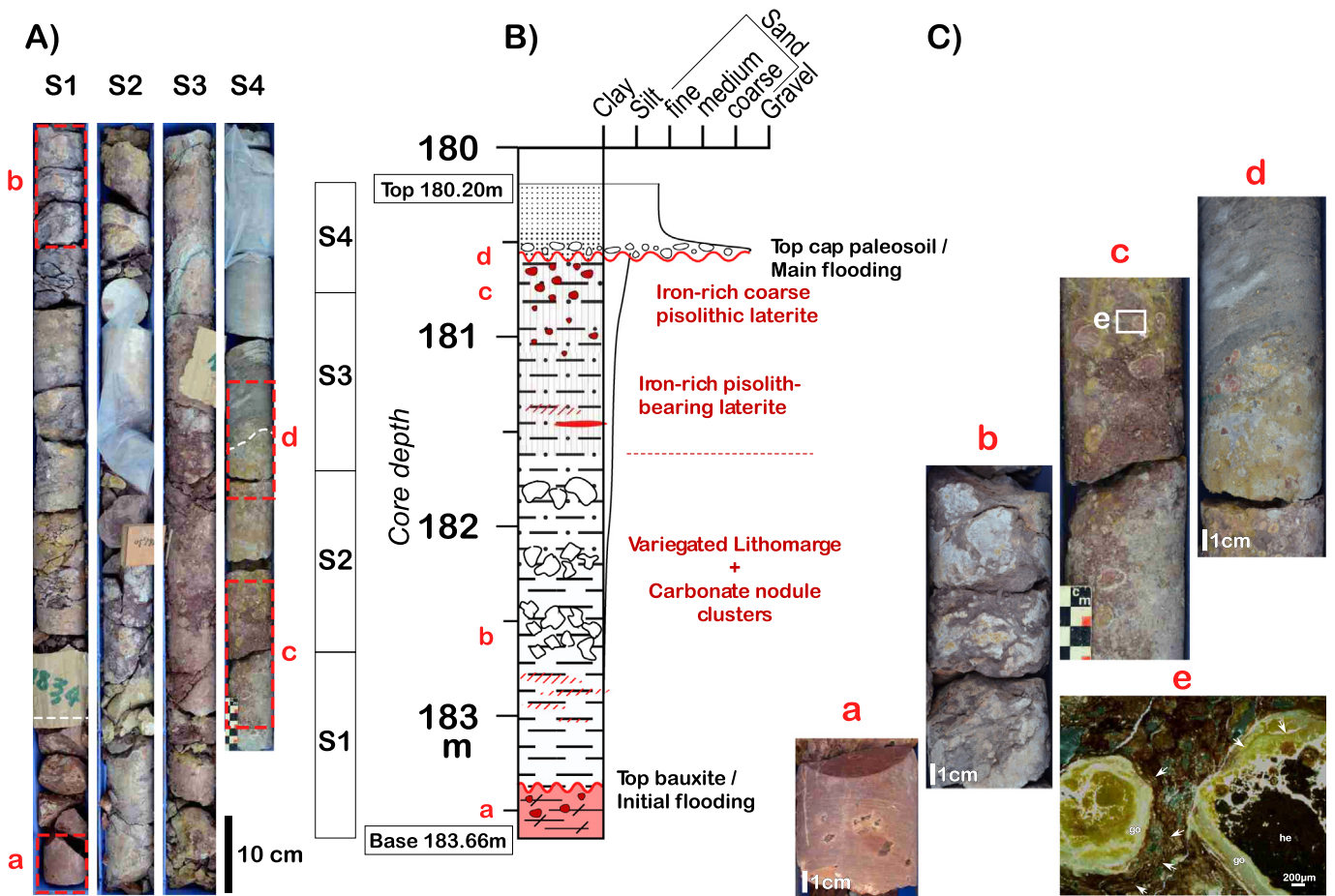


Fig. 7. Detailed architecture of the paleosol capping the bauxite interval: Pedofacies Fp-0. (A) Photographs of the cores, showing the complete lateritic profile sequence on top of the bauxite. (B) Detailed sedimentological section representing the initial coarsening upward flooding sequence, overprinted by an iron-rich sub-lateritic profile. (C) Close-up views of the key facies: (a) Reddish bauxitic claystone (Fb-4); (b) Sub-amalgamated carbonate nodules growing into a dark red claystone; (c) Coarsening and packing upward in situ pisoliths developed into an iron-rich laterite crust pedofacies Fp-0; (d) Irregular erosional surface showing the reworking of iron-rich pisolith nodules by the basal conglomerate. (e) Thin-section showing in situ iron-rich pisoliths from pedofacies Fp-0 (CPRL); white arrows: possible bacterial-mediated envelopes; he: hematite; go: goethite. (For interpretation of the references to color in this figure legend, the reader is referred to the web version of this article.)

a red core, and display an external orange envelope of variable thickness (Fig. 7C-c, C-e), which could indicate the possible inward replacement of hematite after goethite (Fig. 7C-e) as described by Löhr et al. (2013) in the Fraser Coast of Australia. The vertical sequence shows an increase of the iron cortical envelope, and the core of first pisoliths described corresponds to the early synsedimentary facies. This facies progressively passes downward to a variegated clayey fabric including successive indurated white carbonate nodule clusters (Fig. 7A, B, see pedofacies Fp-2 and Fp-3).

The pedofacies Fp-0 shows a vertical progressive organisation and is developed in a dark grey coarsening upward sequence, from carbonate bearing claystone (Fc-1) to clayey siltstone (Fc-2). The clear iron enrichment with associated induration and pisolith development reflects marked vertical leaching, under tropical alternating wet-dry climate (seasonality) conditions, permitting rubification (Duchaufour, 1982; Fitzpatrick, 1988; Schwertmann, 1988). This pedofacies is interpreted as an in situ lateritic profile developed close to a shallow static water table as indicated by the presence of successive carbonate nodules and color variegation. For these reasons, this pedofacies is described as a sub-ferricrete regolith.

4.1.4.2. Variegated to mottled pedofacies (Fp-1). This pedofacies shows a variegated to mottled fabric on the original dark greenish facies of the siliciclastic cover (depositional facies Fc-1, Fc-2 and Fc-3). It is characterized by cm- to dm-scale orange patches, more or less coalescent, and fringed by a dark red drab halo (e.g., Retallack, 1988) (Fig. 8A).

This facies is interpreted as resulting from iron redistribution in the water table fluctuation window, with oxi-hydroxide formation, and represents an early stage of a hydromorphic soil development.

4.1.4.3. Variegated to mottled pedofacies with dispersed mm-size carbonate nodules (Fp-2). The Fp-2 pedofacies is close to the facies Fp-1 from which it differs by the development of dispersed mm-size white carbonate nodules (Fig. 8B) in agreement with the development of a rootlet network, both in the shaley and sandy depositional facies. In thin section, it shows abundant granules of different sizes, separated from the matrix by shrinkage cracks, cemented by spary-calcite (Fig. 8C, D).

This pedofacies is interpreted as early development of a rootlet network in the capillarity fringe, just above the water table, as defined by Wright (1992). The fractured cemented granule (Fig. 8D) indicates sediment contraction occurred by evaporative pumping-driven water loss during subaerial exposure and desiccation, followed by later cementation by down-dip flow into a permanent hydromorphic soil.

4.1.4.4. Variegated to mottled pedofacies with large sub-coalescent carbonate nodules (Fp-3). This pedofacies is defined by sub-coalescent to amalgamated white carbonate nodules forming a hard cemented interval, a few-dm thick. The nodules form a network of carbonate clusters (Fig. 8C) through a variegated to mottled, yellowish to reddish, oxi-hydroxides bearing material. This facies shows a centripetal redistribution of iron oxi-hydroxides around a nucleus leading to the progressive

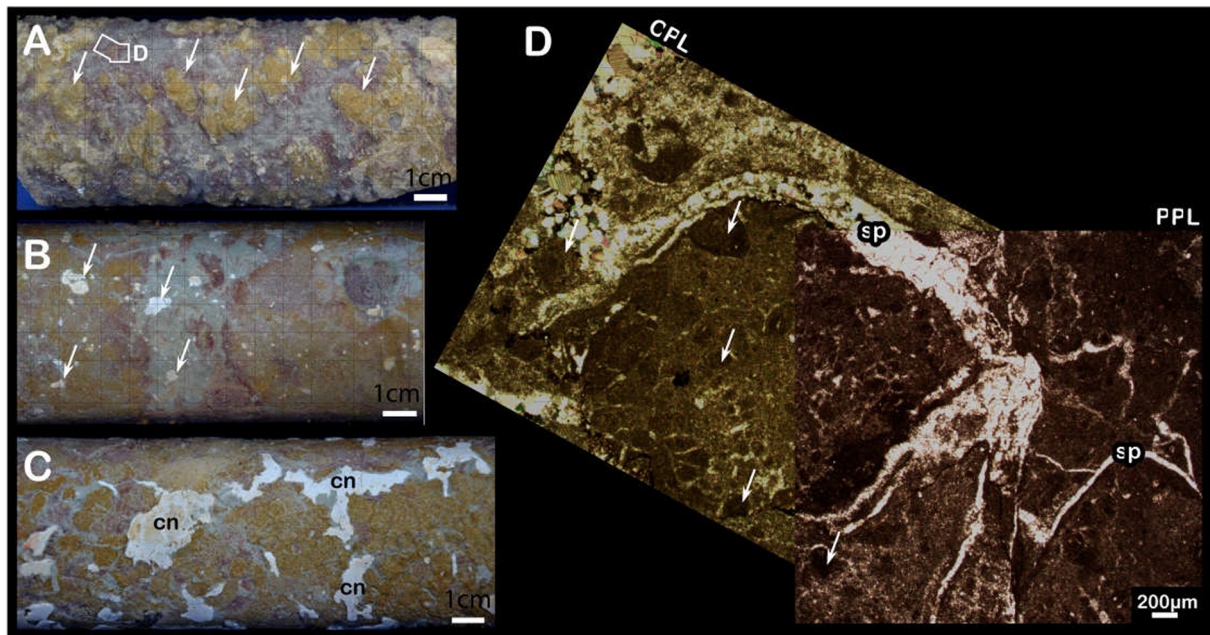


Fig. 8. Macrofacies (as seen on cores) and micropedofacies (thin section, D) developed in the siliciclastic cover. (A) Variegated/mottled pedofacies (Fp-1); white arrows: subnodules dark red halo. (B) Variegated pedofacies showing mm-sized white carbonate nodules (white arrows) (Fp-2). (C) Variegated pedofacies with large sub-coalescent carbonate nodules (Fp-3) forming white large carbonate cluster packages (cn). (D) Thin section of a granulate marl (pedofacies Fp-1) showing abundant granules of varying size (White arrows) separated from the matrix by curved fractures cemented by spary-calcite (sp); Left CPL, right PPL. (For interpretation of the references to color in this figure legend, the reader is referred to the web version of this article.)

differentiation of nodules (corresponding to orange patches; Fig. 8C) that predate the formation of pisoliths.

This pedofacies is interpreted as a more mature hydromorphic soil associated with the development of deep-rooted vegetation and down-dip carbonate leaching, which led to the formation of a groundwater calcrete interval (Wright, 1992) by carbonate nodule amalgamation.

4.1.5. Sedimentary succession stacking pattern and paleoenvironmental interpretation

The sedimentary pile of the representative drillcore 13-OL-184 can be related to three major distinct depositional events (Fig. 2).

First, the fabric of the Upper Jurassic carbonate basement below the bauxite interval is related to subaerial exposure and meteoric karst development, during base level fall. During this phase, the previously formed joints, fractures, veins and stylolites act as preferential pathway for percolation of surficial waters. Millimetre to cm-size endokarstic cavities developed by progressive enlargement at the nodes of the fractures network. In parallel, oxygenated water penetration locally through the fracture network led to subtle marmorisation in the more porous and permeable iron-rich stylolite clusters.

Second, the bauxite interval marks burial of the karstified basement by mass-transported bauxitic material including mudflow (Facies Fb-1), debris-flow (Facies Fb-3) and subsidiary, more diluted, tractive currents (Facies Fb-2). The karst network acts as an efficient sediment trap. No evidence of post-depositional, in situ bauxite evolution (lateritization or paleosols) has been observed in the bauxitic interval. This indicates that the rate at which the material was buried was high enough to avoid subaerial exposure and late leaching. Moreover, the transitional facies succession within the bauxite interval supports continuous sediment transport and deposition. In parallel, the upward grain size increase (pisoliths and iron crust, Facies Fb-3) could reflect an upward intensification of the hydrodynamic regime. The gravity-dominated architecture of the deposits indicates torrential rainfall that triggered the supply of reworked autochthonous laterite bauxite from a proximal source area.

The cover of the bauxite shows a repeated fine-grained siliciclastic series, moderately to highly overprinted by hydromorphic pedogenesis.

The sedimentary succession is dominated by upward coarsening trends whose thickness varies from 2 m to 10 m (Fig. 2). Each trend evolves from dark greenish carbonate bearing claystone or marls (Facies Fc-1) to light greenish homogeneous well-sorted very fine sandstone (Facies Fc-3), through a more or less expanded intermediate facies of greenish pelite to clayey siltstone (Facies Fc-2). Both the abundance of *Teichichnus* burrows and the occurrence of benthic foraminifers in sandstone layers, located 10 m above the top of the bauxite interval, indicate an overall marine environment (Husson, 2013; Knaust, 2018). Nevertheless, both the primary dark green color of the sediment and the deduced moderate energy to standing water are in favor of a restricted, suboxic, paralic to shallow estuarine domain. In particular, the lack of storm deposits suggests isolation from the open sea. In addition, the absence of wood debris, subaquatic channel, crevasse splay or river-flood deposits marks a significant distance from direct continental input. The muddy facies could represent deposition from suspension settling in suboxic standing waters below fairweather wave-base, while the homogeneous very fine sand fraction would support the reworking of a distal deltaic fringe by limited wave action on a shallow shoreface. Here, more oxygenated waters promote intense bioturbation by the settlement of burrowing animals and the associated production of fecal pellets.

The abundance of hydromorphic pedogenesis, ranging from moderate mottling (pedofacies Fp-1) to calcrete nodules amalgamation (pedofacies Fp-3), attests to periodic subaerial exposure and development of swamp to marsh conditions, with rooted vegetation above a shallow fluctuating water table (Wright, 1992). These types of soils represent gleyed to ferric calcisols (i.e., aridisol order according to Mack et al., 1993). They are mainly developed on well-drained soil profiles, in subhumid to semiarid climates (Srivastava et al., 2002; Buol et al., 2003; Schaetzl and Thompson, 2005; Sheldon and Tabor, 2009), characterized by relatively low rainfall (Retallack, 1994; Royer, 1999) and high evapotranspiration (Thornthwaite, 1948; Srivastava et al., 2002). In these conditions, the carbonate fraction was partly leached and transported downward into the soil profile where, with the support of the rooted network, it was precipitated as carbonate nodules close to the water table. The pedofacies changes from Fp-1 to Fp-3 would thus

indicate the increase in duration and maturity, during the soil development (Birkeland, 1999).

The siliciclastic paralic series has been ordered into genetic sequences, ranging in thickness from 2 to 13 m (Fig. 2) and representing the highest resolution sequence as defined by Galloway (1989). These sequences have been in turn grouped into four megasequences, which represent a longer term evolution, but without any constraints about the duration, due to lack of dating (Fig. 2). Genetic sequences consist of superposed shallowing upwards short-term cycles, representing the infilling of the available space during incremental accommodation steps. The regressive trend is also clearly noticeable in the three upper megasequences (MS2, MS3, MS4) which show an overall upward increase of the sand fraction into the individual genetic sequences. Moreover, the three megasequences themselves show an overall upward increase of sand/shale ratios, in agreement with overall progradation of the deltaic source. Only the lower siliciclastic megasequence (MS1) shows a transgressive tendency. Such transgressive-dominated stacking pattern would mark initial marine flooding, at the top of the bauxite deposit, and coeval setting of a restricted submersive marine shelf. However, as clearly evidenced in the sedimentological section (Fig. 2), there is no direct link between the genetic sequences and the pedogenic profiles, which indicates that successive soil profiles partly overlapped, giving rise to composite/cumulative paleosols, resulting from slow and steady sedimentation rates (Bown and Kraus, 1987; Kraus, 1999).

4.2. Mineralogical units

Both bulk XRD and clay mineralogy allow for better constraints on sedimentological analysis and in particular on depositional conditions.

4.2.1. Whole rock mineralogy

Bulk XRD analysis of the bauxite interval shows the presence of boehmite and hematite in samples B1 and B2 (Fb2 and Fb3 facies respectively; Fig. 9A). Sample B3 located on the top of the bauxite interval, corresponding to the Fb4 facies, also shows the appearance of kaolinite associated with boehmite and hematite (sample B3, Fig. 9A).

The siliciclastic cover is mainly composed of quartz, calcite and clay phases. The lower part of the siliciclastic series (samples K3 to K5; Fig. 9A) is dominated by calcite with minor contribution of quartz, whereas the upper part (samples K8 to K13; Fig. 9A) presents large quartz contributions.

4.2.2. Clay mineralogy

Clay-rich samples were investigated with XRD considering the fraction below 2 μm (Fig. 9B). In the bauxite interval, only the top of the profile shows the presence of clay exclusively composed of kaolinite (sample B3). In the siliciclastic cover, the clay mineral assemblage is dominated by either kaolinite (7 \AA phase) or smectite (14.2 to 14.9 \AA phase) in association with 10 \AA phases, corresponding to illite or micas. Significant evolution occurs in the siliciclastic cover succession. The kaolinite 7 \AA peak is clearly developed at the base of the series than upwards (K1 to K5; Fig. 9C), whereas smectite peak intensity is low at the base of the siliciclastic cover, but increases upwards and is well represented in the upper samples (K8 to K13, Fig. 9C). The smectite-dominated upper interval is associated with the appearance of a 10 \AA phase (Fig. 9C). In order to distinguish additional clay species, such as chlorite or I/S mixed layer, the high smectite content sample K11 was analyzed, using ethylene glycol treatment (Fig. 10). The resulting diffractogram shows expandable smectite passing from 14.9 d-scale to 16.7 d-scale (Fig. 10). No peak in the 14 d-scale was observed, or in any other air-dried diffractograms through the succession. This confirms the absence of chlorite in the sedimentary succession. Finally, the glycolated smectite peaks d001 at 16.7 \AA , d002 at 8.45 \AA and d003 at 5.5 \AA indicate the absence of a I/S mixed layer.

4.2.3. Characterization of the mineralogical units

According to bulk and clay mineralogy analysis, we distinguish four successive mineralogical units from the base to the top of the succession.

Unit 1 (189.75–183.80 m) is represented by the B1 (189.50 m) and B2 (186.00 m) samples of the bauxite interval (Fig. 9C). This hematite and boehmite-dominated mineral unit corresponds to facies Fb3 and Fb2. This mineral assemblage is consistent with the microfacies analysis and characterizes the deposition of detrital bauxite.

Unit 2 is located on top of the bauxite interval (183.80–183.55 m; Fig. 9C) and corresponds to the Fb4 facies. The mineral association is strongly dominated by kaolinite with subordinate boehmite and hematite which is in agreement with the described clayey matrix that includes scarce pisoliths and iron-rich crust clasts.

Unit 3 (183.55–180.45 m), located in the siliciclastic cover, corresponds to the cap-paleosol that overlies the bauxite interval (Fig. 9C). This mineral zone shows a high intensity of the kaolinite 7 \AA peak associated with the smectite d001 peak, whose intensity strongly increases towards the top of the unit. Bulk XRD reflects low quartz content and abundant calcite. The transition from Unit 3 to Unit 4 correlates with the paleosol, which marks the overall change from a high kaolinite-peak intensity unit to the dominance of smectitic peak to the top of the drillcore.

Unit 4 (180.45–0 m) corresponds to the main siliciclastic cover interval (Fig. 9C). The mineral assemblage of this unit is dominated by smectite associated with some kaolinite. The latter shows a relative peak intensity decreasing towards the top of the succession. The 10 \AA -phase was also evidenced only in this unit. The bulk XRD diffractograms show the dominance of quartz compared to the previous units.

4.2.4. Interpretation of the mineralogical units

The four mineralogical units distinguished in the drillcore succession include both detrital and authigenic fractions that provide constraints on the nature of the source area, and the conditions of weathering and transport. The mineralogy and fabric of in situ or reworked paleosol profiles are weathering-dependent (Sheldon and Tabor, 2009). In particular, the intense dissolution of detrital silicate minerals from the parent material, during vadose downward percolation, leads to the crystallization of new phases, which are characterized by (i) high content in relatively immobile cations (Al, Si, Fe, Ti), and (ii) variable preservation of soluble cations (Na, K, Mg, etc.) depending on hydro-morphic and drainage conditions. The consequence of this dissolution-crystallization process is the authigenesis of soil-derived species (in particular, kaolinite and smectite), and/or Fe, Al and Ti oxides and hydroxides (Schwertmann, 1988).

Mineralogical Unit 1 is relatively enriched in Al hydroxide. The presence of boehmite suggests a strong hydrolyzed parent material that sourced this allochthonous bauxite interval. Mineralogical Unit 2 is characterized by kaolinite in association with boehmite and hematite, without a distinctive paleosol zonation. Moreover, Unit 2 displays the same fabric as the underlying bauxite, which suggests either the dismantling of a less resistant hydrolyzed parent profile, or mixing of two different sources that allows for preservation of both boehmite and silica in kaolinite. These two hypotheses imply the deep reworking of successive and distinct horizons of a primary autochthonous lateritic profile and its transport and trapping in the same karstic network.

Detrital clay mineral assemblages derived from nearshore marine deposits in the siliciclastic cover (Units 3 and 4) can provide important information on past changes in weathering regime on the adjacent continent, which in turn predominantly depends on overall climatic regime. However, palaeoclimatic interpretation of clay mineral records is hampered by a variety of factors, including marine or continental authigenesis and diagenetic alteration during burial (Thiry, 2000; Ruffell et al., 2002). Interpreting the clay mineral successions in terms of paleoenvironment requires evaluation of the influence of diagenesis. Occurrence of smectite and absence of I/S mixed layers in the siliciclastic

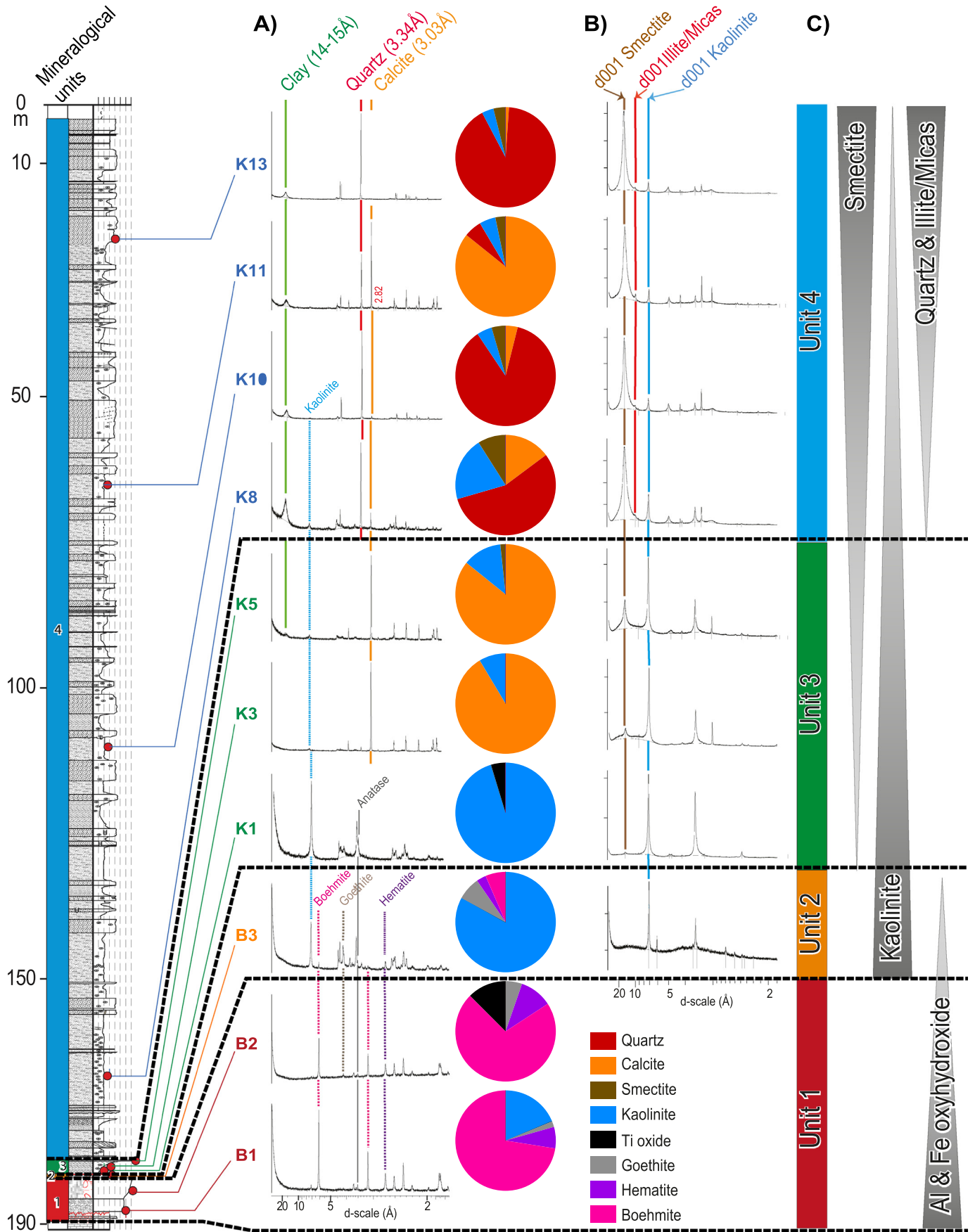


Fig. 9. XRD diffractograms of representative samples through the Villeveyrac sedimentary succession. (A) Bulk mineralogy showing iron and aluminium oxy-hydroxides dominated Units 1 and 2, kaolinite and calcite dominated Unit 3 and quartz dominated Unit 4. (B) Clay mineralogy (<2 μm fraction) showing a kaolinite dominated Unit 3 and a smectite dominated Unit 4, associated with the appearance of 10A phases (illite/micas). (C) Synthetic representation of the mineralogical composition of the 4 units.

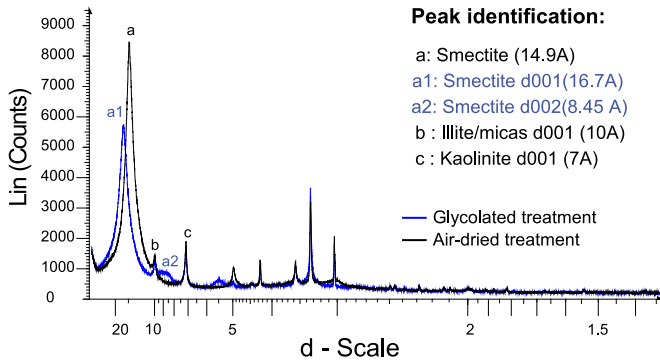


Fig. 10. Air-dried and glycolated XRD pattern of the <2 μm fraction of the marly K11 sample, which confirms the absence of diagenetic mixed layer clay.

cover indicate negligible influence of burial diagenesis. Indeed these minerals are very sensitive to temperature increase, with onset of illitization at about 60 °C, inducing the progressive transformation of IS R0 into I/S R1, then R3, and finally into illite (Kübler and Jaboyedoff, 2000; Kübler and Goy-Eggenberger, 2001; Środoń, 2009). In the studied section, the illitization process is considered as subsidiary, because of the absence of correlation between smectite and illite peak intensity variations throughout the succession. This is consistent with weak early and burial diagenetic clay authigenesis, which suggests that the observed smectite, as well as kaolinite and 10 Å phase, should mainly have a detrital origin and can therefore be interpreted as the result of paleoenvironment changes.

Unit 3 shows the highest kaolinite peak intensity that suggests pedogenetic authigenesis under warm and humid tropical conditions suitable for high rates of chemical weathering and strong bedrock leaching under average annual temperatures above 25 °C (Gaucher, 1981; Chamley, 1989; Hallam et al., 1991; Righi and Meunier, 1995; Ruffell et al., 2002). However, this mineral may be also reworked together with primary minerals (e.g., illite) from ancient kaolinite-bearing sedimentary rocks (Deconinck et al., 1991). In this case, kaolinite alone cannot be used as evidence for the existence of a humid climate. Coupling or decoupling in the variation of primary minerals and of kaolinite, however, may help distinguish a pedogenic or reworked origin, thereby indicating the reliability of kaolinite as a palaeoclimate indicator. Since these two minerals do not vary in a similar way in units 2, 3 and 4, they probably have different origins. The upwards decrease of kaolinite-peak intensity from the Fp-1 to Fp-0 pedogenetic facies, and also towards more mature soils, indicates that kaolinite is not a result of early pedogenesis overprint. Kaolinite is also interpreted as detrital in origin and product in pedogenetic blankets in the source area in Units 3 and 4.

Unit 4 shows an increase in smectite peak intensity, coeval with a decrease in kaolinite peak intensity and with the appearance of 10 Å phases and detrital quartz. In this way, the evolution through Units 3 and 4 may reflect the transition towards a drier climate with rainfall seasonality, inducing mechanical erosion of fresh bedrock, associated with poorly drained soil in the source area (Deconinck and Chamley, 1995). The appearance of mica or illite 10 Å phases indicates active mechanical erosion in the source area and limited soil formation. This detrital clay minerals in relation to low hydrolyzing conditions confirms the tendency towards a drier climate (Chamley, 1989; Weaver, 1989; Ruffell et al., 2002).

However, other controls independent of climate can affect this clay association evolution, such as a change in source-area lithology, tectonic regime or base-level evolution (Chamley, 1989; Deconinck and Chamley, 1995). Therefore, the first-order evolution of the clay mineral association through the siliciclastic cover sequence can be interpreted as the result of (i) decrease of weathering condition with time, that can result from climate changes, (ii) changes of soil in eroded source

area (i.e., downstream versus upstream catchment), and/or (iii) tectonic control. In any case, the upward evolution of the fine-grained mineral fraction of the drillcore section, from authigenic-dominated at the base (Unit 1) to detrital-dominated to the top (Unit 4), with a mixed composition in the intermediate interval (Units 2 and 3) implies a progressive change of weathering conditions in the basin. The origin of changes in weathering conditions can be specified in light of geochemical data.

4.3. Geochemical signatures of the mineralogical units

Geochemical analyses across the major mineralogical transition described above help to identify the controlling processes (Fig. 11).

4.3.1. Geochemical characterization of the four units

As expected, Unit 1 shows the lowest contents of SiO₂ and CaO together with relatively high contents of Al₂O₃ and TiO₂ (Fig. 11). The bauxite trapped into the endokarstic cavities of the Jurassic basement displays a lower content of Al₂O₃ and TiO₂ and higher content of silica.

Unit 2 shows a relative decrease in Al₂O₃ and TiO₂ and a correlative increase in Fe₂O₃ and SiO₂ consistent with the presence of kaolinite, evidenced by XRD analyses of the <2 μm fraction.

Unit 3 marks a major change in chemical composition with an increase in SiO₂ content. Al₂O₃ and TiO₂ decrease through this unit, whereas Fe₂O₃ is very low and constant. This evolution is related to the disappearance of iron oxides and aluminium hydroxides. This unit is also characterized by very high CaO content, linked to the abundance of marly facies in this interval and calcite evidenced by XRD analysis.

Unit 4 shows a significant increase in SiO₂ content corresponding to the quartz fraction evidenced the XRD analysis. CaO remains relatively low and constant, in particular because the analysis was done outside the carbonate pedogenetic nodules. Fe₂O₃ remains low in this unit.

4.3.2. Interpretation of geochemical evolution

The Villeveyrac bauxite geochemistry is dominated by TiO₂, Al₂O₃, FeO and SiO₂, as is describe in the Spinazzola karst bauxite (Mongelli et al., 2014). These chemical elements are indicative of conditions of weathering and transport, depending on their relative stability (Valeton, 1972). Titanium, in particular, is considered as invariant in the mass-balance calculation, because of its very low mobility during weathering (Nesbitt, 1979; Scheepers and Rozendaal, 1993). In the recovered section, the TiO₂ vs Al₂O₃ diagram shows a strong correlation (R² = 0.8; Fig. 11B), suggesting that, during weathering, aluminium has the same immobile behavior as titanium (Mongelli et al., 2017). Such coeval evolution remains the same for the bauxite interval where the TiO₂ and Al₂O₃ content is highest, and for the siliciclastic cover, where it decreases drastically in Unit 3, and remains low and constant in Unit 4. This indicates the dilution and stabilization, respectively, of the detrital fraction. The juxtaposition of the same trend for the four units suggests that parent rocks in the source area remain the same, with only a difference in weathering intensity.

In addition, the SiO₂ vs TiO₂ diagram helps to constrain the weathering processes in the source area (Fig. 11C). For Unit 1, the lowest SiO₂ content relative to the highest TiO₂ content is indicative of intense hydrolyzing processes, with leaching and evacuation of the silica from the pedologic profile, and coeval concentration of the insoluble fraction (TiO₂) and oxide and hydroxide authigenesis. In the case of Unit 4, the relative abundance of SiO₂ and depletion of the insoluble fraction (TiO₂; Fig. 11C) indicate upstream preservation of silica, under milder hydrolyzing conditions. In the case of Unit 2, the SiO₂/TiO₂ ratio follows the same trend and is close to that of Unit 3 (Fig. 11C), which suggests the same fractionation process, without any in situ diagenetic authigenesis. Furthermore, this confirms the detrital origin of the kaolinite in the basin. Finally, Unit 3 shows an intermediate chemical composition (Fig. 11A) with a progressive decrease of TiO₂ content accompanied by a sharp increase of SiO₂ at the base of the unit followed

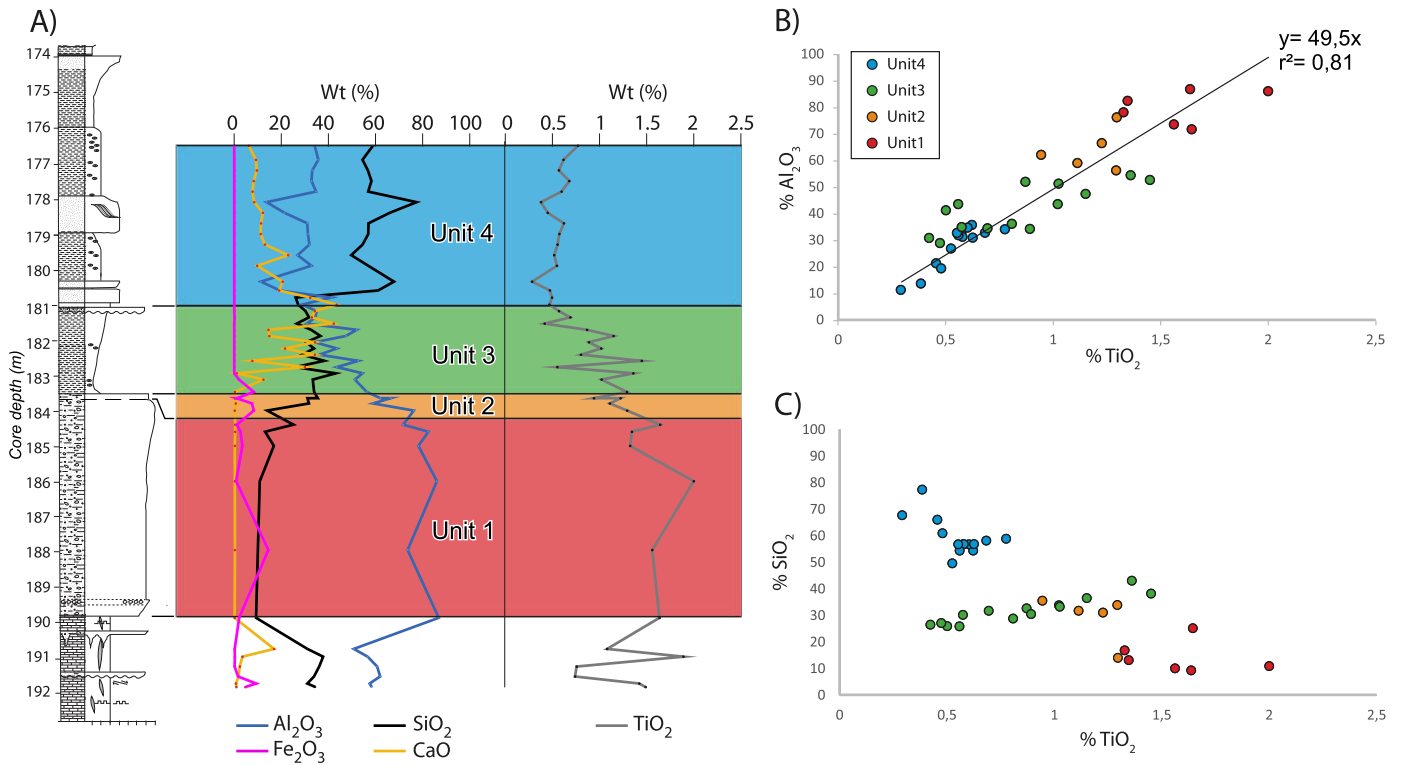


Fig. 11. Variations of the major oxides (Al_2O_3 , Fe_2O_3 , SiO_2 , CaO and TiO_2) in the Villeveyrac sedimentary succession. (A) The mineralogical units (same color-code as in Fig. 9) show a decrease of immobile elements (aluminium and titanium) associated with an increase of mobile element (silicium) towards the top. (B) Cross-plot of Al_2O_3 versus TiO_2 ; the colors are referred to the mineralogical units. (C) Plot of $\text{SiO}_2/\text{Al}_2\text{O}_3$ that shows an increase of mobile element from the Unit 1 to the Unit 4.

by an upward slight decrease. This unit can be interpreted as an abrupt change of depositional conditions from the input of silt and clay, which is later affected by in situ limited rubification leading to the development of a sub-ferricrete paleosol.

5. Discussion

The mid-Cretaceous succession of the Villeveyrac Basin records major changes in sedimentation processes, pedofacies and sediment mineralogy and geochemistry, shown by the four depositional units relating to a decrease of weathering intensity. This results from a balance between forcing parameters that control mechanical erosion versus chemical weathering. In this section, we discuss and discriminate the recorded signals of the source material and tectonic and climate changes during deposition of this succession.

5.1. Origin of the Villeveyrac bauxite ore deposit

Based on facies analysis, highlighting the mass-transported architecture of the deposits and the abundance of iron-crust clasts and broken pisoliths, and following the works of Combes (1969, 1973, 1984), we confirm the allochthonous origin of the Villeveyrac bauxite ore deposit, sensu Bardossy and Combes (1999). The allochthonous karstic bauxite deposit of Villeveyrac shows multiple stacked massive deposits with different grain size and matrix contents, all including broken blocks of iron crust and pisoliths indicating an overall mechanical transportation compatible with mass-transport processes and more rarely tractive currents. The mineralogical signal of Villeveyrac allochthonous bauxite is close to the allochthonous Salento-type bauxite describe in Italy (Mongelli et al., 2015) with a boehmite dominated bauxite depleted in kaolinite. The mineralogical and geochemical analyses provide a more detailed signature of the parent-source material. Units 1 and 2 located in the bauxitic interval are characterized by a decrease of Al_2O_3 and TiO_2 contents associated with the appearance of kaolinite in Unit 2,

indicating a decrease of immobile elements inside the deposit. Thus, Unit 1 records the mineralogical and geochemical signal of an autochthonous lateritic residuum cover corresponding to the most intense weathered horizon composed of iron oxides and Al hydroxides (Butt et al., 2000). Unit 2 is interpreted as the dismantling of a mottled horizon, with the preservation of iron oxide and kaolinite, associated with the demise of Al hydroxide (Aleva, 1994; Butt et al., 2000). Coupled sedimentology, mineralogy and geochemistry results indicate that the Villeveyrac bauxite also shows a well preserved signal of the superposed lateritic horizons. No consistent vertical geochemical trend has been observed, which could have indicated in situ, post-depositional downward leaching. The detrital bauxite did not undergo any secondary, post-depositional lateritic evolution. This suggests relatively quick deposition and sealing of the detrital bauxite interval, which accounts for the exceptional preservation of signatures of the different parent rocks. The Villeveyrac bauxite ore is therefore a typical allochthonous karst bauxite deposit fed by a proximal source and trapped in a karst system. The vicinity of the source of the detrital bauxite is testified by transport implying a high slope gradient and heavy rainstorms on close low-vegetated bordering reliefs that triggered unconfined debris-flows to mud-flows. Following the work of Iverson (1997), the traveled distance for a debris-flow avalanche (L) is a function of the vertical elevation of the debris-flow source above the deposit (H) and the dimensionless net resistance coefficient (R) expressed by: $1/R = L/H$. A traveled distance for a vertical elevation of about 500 m can be estimated between 12 km in the case a 10^9m^3 mudflow with $1/R = 25$ as in the case of the Mount Rainer Osceola mudflow (Vallance and Scott, 1997), and 3 km for a 10^5m^3 landslide with $1/R = 6$ like that observed at Mount Thomas in New Zealand (Pierson, 1980). These data confirm that the initial lateritic source of the Villeveyrac bauxite was a few kilometers to a few tens of kilometers from the depocenter.

Based on LA-ICP-MS U-Pb dating on detrital zircons from bauxite ore deposits including the Villeveyrac basin, Marchand et al. (2020) proposed a dual source for the parentrocks of the bauxites. First, a

significant proportion of Paleozoic ages, together with a decrease away from the Variscan basement outcrops indicate a Variscan source. Second, a large proportion of Late Mesoproterozoic to Archean detrital zircon ages, which are regionally distributed, cannot be accounted for by a source from the Variscan basement. This suggests another source, derived from the bauxitisation of a regionally extensive sedimentary cover, involving multiple recycling of inherited old zircons. For these authors, the regional sedimentary source is consistent with the removal of the lateritized Valanginian marly sequence that represents the thickest extensive clayey, i.e., aluminous-rich deposit that is younger than the Late Jurassic bauxite wall and older than the Albian bauxite (Barbarand et al., 2001; Séranne et al., 2002).

5.2. Role of slope gradient and differential mobility on the topographic surface

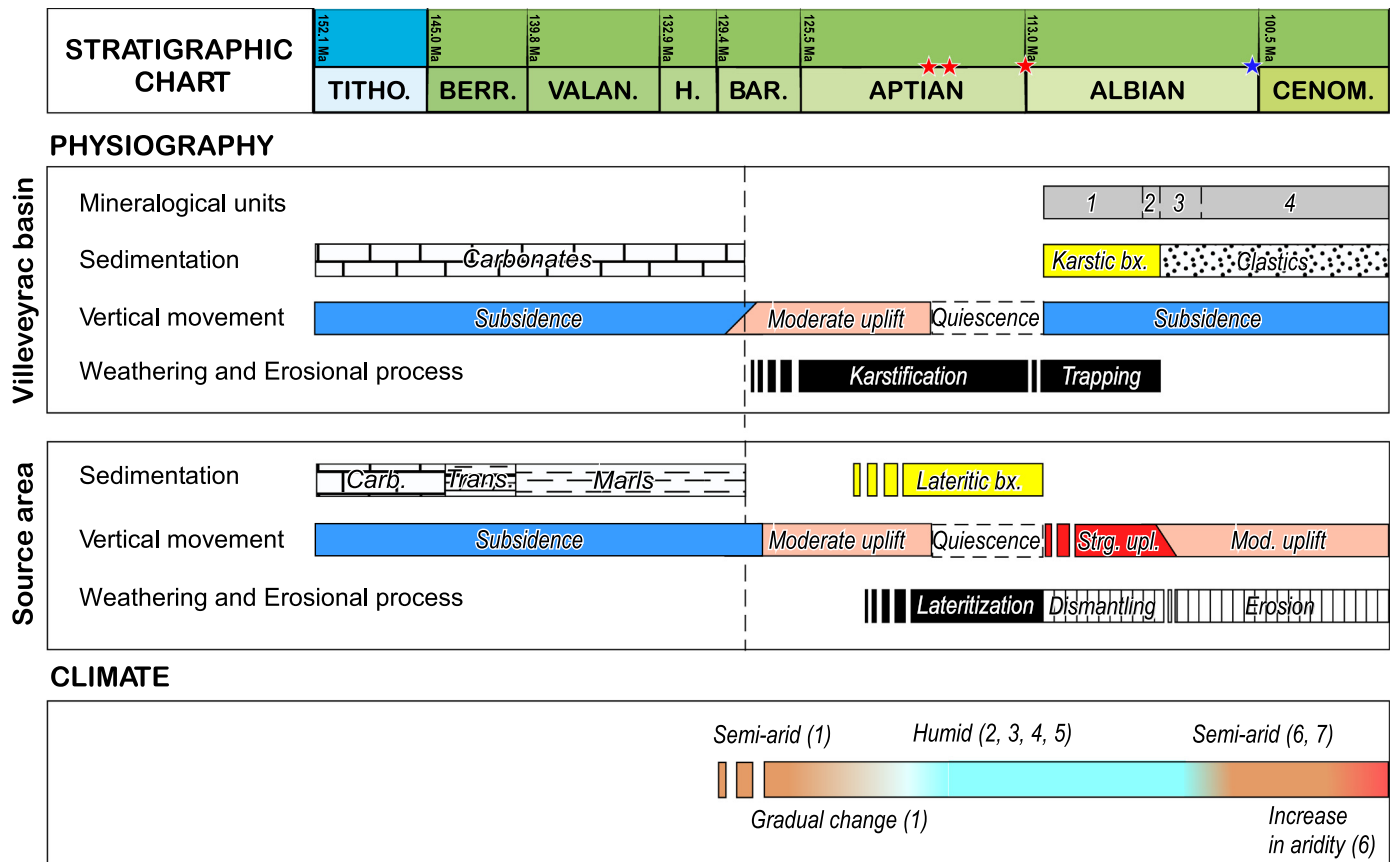
The allochthonous karstic bauxite results from two separate processes: (1) in situ hydrolysis of an Al-rich mother rocks, and (2) mechanical erosion and export of the resulting autochthonous lateritic profile. This points towards two different geomorphic and drainage conditions.

First, the development of the lateritic profile is consistent with slow and gradual base-level fall, under stable climatic conditions (Wyns et al., 2003). Such conditions favor vertical percolation leading to leaching and basinward exportation of alkalis, earth alkali and silica elements; with coeval enrichment in insoluble oxides and hydroxides in the profile. Conversely, limited incision and denudation are consistent with tectonic quiescence that preserves the stability of the evolving lateritic

profile (Bardossy, 1982; Aleva, 1994). The resulting surface would have been close to an extensive etchplain-type planation surface (Migon, 2004). The downstream preservation of bauxite in the karst and marine cover implies base-level rise. The detrital kaolinite on top of the bauxite interval (Unit 2) may reflect erosion of the mottled zone at the base of the lateritic profile (Valeton, 1972). Thus, we suggest that bauxite deposition was first governed by rapid uplift of the catchment and associated slope gradient increase, between a downstream karst trap and upstream lateritic etchplain. Dismantling of the insitu bauxite reflects differential tectonic uplift of the hinterland, during the mid-Cretaceous (Barbarand et al., 2001; Peyaud et al., 2005). Differential vertical movements across southern France are related to contemporaneous opening of the Bay of Biscay and drifting of the Iberia plate (e.g., Lagabrielle et al., 2010; Tavani et al., 2018), which is expressed in the study area by uplift and erosion of the so-called "Durancian Isthmus".

Units 1 and 2 mark the emplacement of debris-flows and mudflows whereas the transition between Units 2 and 3 reflects cessation of reworking and deposition. Units 3 and 4 correspond to clayey marl suspension settling in a quiet paralic environment, with periodic fine to very fine sand input. This is consistent with continuous base-level rise and decrease in catchment slope gradient. The repeated stacking of shallowing upward sequences marks the persistence of paralic environments and supports a decrease of tectonic activity. Thus, the Latest Albian to Cenomanian siliciclastic cover describes a continuous transgressive trend with a balance of subsidence and detrital input.

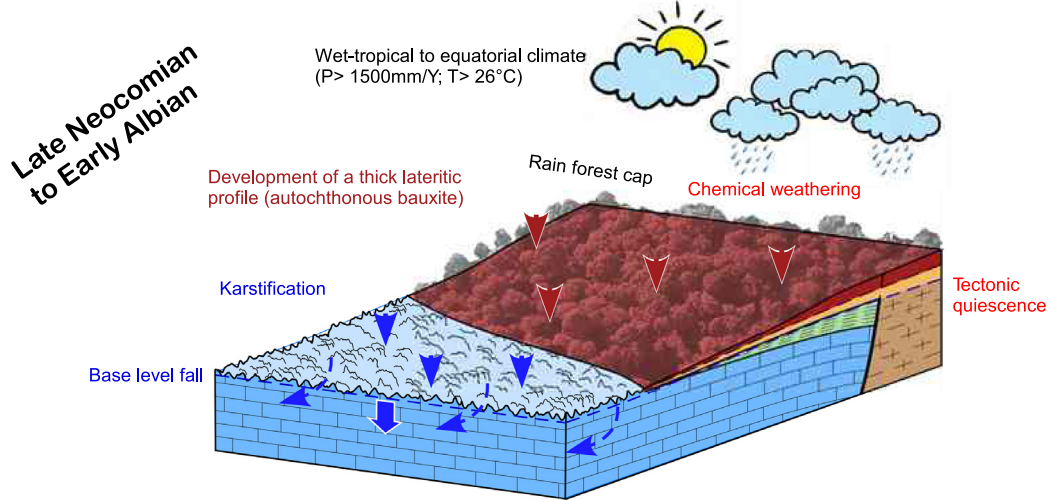
The coeval decrease of differential uplift between the drainage basin and the depocenter, with a transgressive tendency, cannot lead to the observed mineralogical change between Units 1 and 4. This is more in



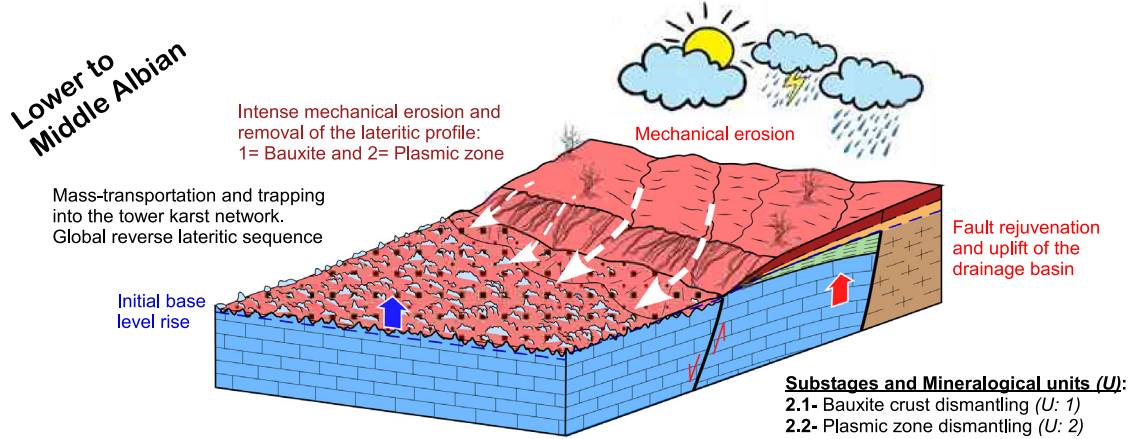
Absolute ages : ★ Youngest detrital zircon grains (U/Pb): 118 - 117 - 113 Ma (Marchand et al., 2020); ★ Foraminifera: Vraconian (Husson et al. 2013)

Fig. 12. Chart of a tentative geohistory reconstruction, from the Tithonic through to Cenomanian (top frame) in the Villeveyrac basin (second frame) and source area (second frame) (modified from Marchand, 2019). The Global climate interpretation (lower frame) are from: (1) Ruffell and Worden (2000); (2) Heimhofer et al. (2008), (3) Ludvigson et al. (2015); (4) Suarez et al. (2011); (5) Stein et al. (2012); (6) Giraud et al. (2013); Corentin et al. (2019).

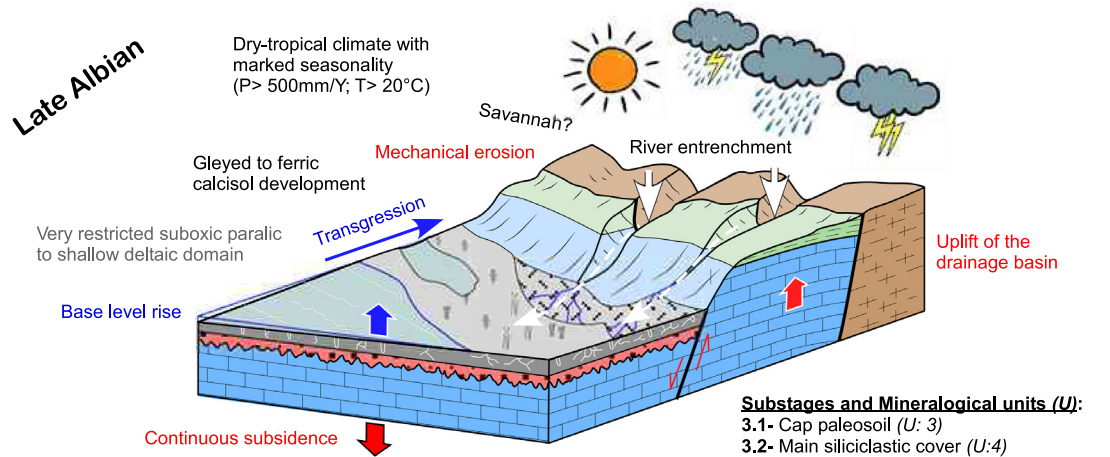
Stage 1 - Regional quiescence: Intense karstification and lateritization



Stage 2 - Tectonic rejuvenation and uplift at climate transition: Autochthonous bauxite dismantling and trapping.



Stage 3 - Major climate change and regional transgression: Mechanical erosion and detrital input on a restricted shallow shelf.



Allochthonous bauxite (Albian)	Siliciclastic cover (Late Albian)	Fine bioturbated sandstones	Teichichnus burrows
Early Cretaceous marls (Neocomian)	Claystone and siltstone	Plasmic zone (Kaolinite)	Hydromorphic paleosoils and pedogenetic nodules
Jurassic limestones	Lateritic profile (Albian)	Autochthonous bauxite	
Crystalline basement			

Fig. 13. Synthetic representation of the depositional environments and forcing factors, which controlled the development (stage 1), dismantling (stage 2), and trapping and sealing (stage 3) of the bauxite deposits of the Villeveyrac Basin (see the text for detailed comment).

accordance with a weathering decrease related to climate change towards less hydrolyzing conditions.

5.3. Evidence of climatic changes during the Aptian-Albian

Thanks to the pedofacies and mineralogical characterization, climate conditions during the Albian can be specified. The bauxite interval records a relatively stable, wet tropical to equatorial climate, as demonstrated by the predominance of allitization (Duchaufour, 1982; Pédro, 1984). This marks the complete leaching of mobile elements from the regolith and vertical stacking of iron and aluminium oxo-hydroxides, with a plasmic kaolinite-rich zone at the base of the profile (Units 1 and 2).

The global warm-humid conditions that prevailed during the Aptian were demonstrated by numerous authors (Ruffell and Worden, 2000; Heimhofer et al., 2008; Suarez et al., 2011; Stein et al., 2012; Giraud et al., 2013; Ludvigson et al., 2015; Coarentin et al., 2019) (Fig. 12). In particular, based on the interpretation of spectral Gamma-Ray data (K, U, Th) from mid-Cretaceous deposits of southern England and southern France, Ruffell and Worden (2000) showed a clear link between Th and K-U partitioning and a change in weathering conditions attributed to the transition between semi-arid climate from the Barremian to early Aptian and wetter conditions during the Mid-Aptian.

Based on $\delta^{18}\text{O}$ signature of pedogenetic carbonates, Suarez et al. (2011) and Föllmi (2012) suggest a generally humid climate in the northern hemisphere, including the southern France, accompanied by intense precipitation, during most of the Aptian and earliest Albian. Similarly, the appearance of kaolinite on the northern Tethyan carbonate platform during the early Aptian has been considered as a change towards more humid climate conditions (Stein et al., 2012).

The top of the Unit 3, which caps the bauxite interval, shows the first in situ soil developed on the basal clayey sequence (Fig. 7). This yellowish-red regolith is interpreted as a sub-ferricrete paleosol consistent with rubification under an alternating wet-dry tropical climate (Duchaufour, 1982; Fitzpatrick, 1988; Schwertmann, 1988). It is therefore considered as a capformed at the end of the last oxidative subaerial exposure, during the regional transgressive cycle.

After the sub-ferricrete interval, no more iron-rich paleosol appears in the sequence, and deposits of the clay association shows a progressive change from kaolinite to smectite inherited from the source area. Smectite peak high intensity indicates that rainfall and drainage were not sufficient to eliminate all the leached elements, which suggests an alternating wet-dry topical climate in the source area. Hydromorphic pedogenesis extensively developed in the rest of the siliciclastic cover (Unit 4), which is characterized by a gleyed to ferric calcisol (Mack et al., 1993), showing the persistence of the same climatic conditions. The appearance of illite and micas, as well as feldspar on the sandstone lithofacies throughout Unit 4, records hydrolysis in the upstream regolith. In the basin, the stable wet-dry tropical climate, combined with a shallow fluctuating water table led to the setting of the highly pedogenetic sediment succession (Fig. 12).

During the middle late Albian, smectite-rich sedimentation in the Vocontian basin (Fig. 1B) and paleobotanical data suggest a latitudinal expansion of the semi-arid climatic belt, which could have continued to the late Albian (Coarentin et al., 2019). In particular, the close boundaries between the semi-arid and warm-humid belt, defined by Chumakov et al. (1995), are consistent with the subtle climatic fluctuation observed in the Villeveyrac basin. Cenomanian aridification is confirmed by Giraud et al. (2013) who showed that, during the Cenomanian and until the Mid Cenomanian event 1a (MCE1a), a drier climate existed in the Vocontian Basin (Fig. 1B).

6. Conclusions

The Villeveyrac basin sedimentary succession, including the Jurassic karstified basement, the Albian allochthonous karst bauxite and its clastic

cover represent a period of a about thirty millions years-long time that records an autochthonous laterite bauxite formation, dismantling, trapping and sealing by paralic sediments. The facies analysis, mineralogy and geochemistry of this singular depositional sequence indicates a first order tectonic control following by a first order climate change. Three main stages are distinguished including second order, facies-related, substages reflecting physiographic changes between the drainage basin and the depocenter (Figs. 12, 13).

Stage 1- Regional quiescence: Intense karstification and lateritization

Progressive "Isthme Durancien" subaerial exposure of the Variscan crystalline basement and Neocomian marls, under wet tropical/equatorial conditions, led to the development of a thick insitu bauxite profile during a tectonically stable period. During the late Neocomian-early Albian, an active karst was developed. The upstream domain can be considered as an extensive etchplain-type planation surface with chemical weathering during base-level fall.

Stage 2- Tectonic rejuvenation and rapid uplift of the source area during climate transition: Autochthonous bauxite dismantling and trapping

Differential uplift of the drainage basin led to the widespread dismantling and erosion of the autochthonous lateritic bauxite cover. The reworked laterites were transported as mud- to debris-flows, and trapped in the karst. Under persistent wet tropical conditions, the increase of slope gradient favored mechanical erosion. During this period, base-level rise led to the preservation of the detrital bauxite in the karstic trap. The input of boehmite and hematite-goethite material (Unit 1) passing upwards to kaolinite-dominated facies (Units 2 and 3) reveals progressive stripping of lateritic in the hinterland and reverse stacking, as a detrital sequence, into the karstic trap.

Stage 3- Major climate turnover during regional transgression: Mechanical erosion and steady subsidence rate: paralic sedimentation

The sub-ferricrete paleosol capping the bauxite interval accounts for both the change in depositional conditions, and aridification with rainfall seasonality. After transgression and during the rest of the late Albian, stable climate conditions, with decreasing uplift of the source area, led to the stacking of fine-grained siliciclastic sequences into an overall paralic to swamp transgressive cycle.

Declaration of competing interest

The authors declare that they have no known competing financial interests or personal relationships that could have appeared to influence the work reported in this paper.

Acknowledgements

We are grateful to Dorian Fourrier from the SODICAPEI (Vicat Group) who allowed us to analyze the drillcore and take samples. We also thank Christophe Nevado and Doriane Delmas (Géosciences Montpellier) for the realization of the thin sections. ML and MS thank their mentor P.J. Combes for his precious expertise on bauxites. The study was financed by IMT Mines Alès and Géosciences Montpellier.

References

- Alabouvette, B., Demange, M., Guérangés-Lozes, J., Ambert, P., 2003. Notice explicative, carte géologique de France (1/250,000), feuille Montpellier (38) (Bureau de Recherches Géologiques et Minières).
- Aleva, G.J.J., 1994. Laterites: Concepts, Geology, Morphology and Chemistry. International Soil Reference and Information Centre. Wageningen, Netherlands 169 pp.
- Anand, R.R., Verrall, M., 2011. Biological origin of minerals in pisoliths in the Darling Range of Western Australia. *Aust. J. Earth Sci.* 58, 823–833.
- Arnaud-Vanneau, Arnaud, Charollais, Conrad, Cotillon, Ferry, Masse, Peyberrière, 1979. Paleogeography of the urgonian limestones of the Southern France. *Geobios* 12, 363–383.
- Arthur, M.A., Dean, W.E., Schlanger, S.O., 1985. Variations in the global carbon cycle during the Cretaceous related to climate, volcanism, and changes in atmospheric CO₂. In: Sundquist, E.T., Broecker, W.S. (Eds.), *The Carbon Cycle and Atmospheric CO₂*; Natural

- Variations Archean to Present. Geophysical Monograph Series, 32, Washington, D.C., pp. 504–529.
- Barbarand, J., Lucazeau, F., Pagel, M., S eranne, M., 2001. Burial and exhumation history of the south-eastern Massif Central (France) constrained by apatite fission-track thermochronology. *Tectonophysics* 335, 275–290.
- Bardossy, G., 1982. Karst Bauxites, Bauxite Deposits on Carbonate Rocks. *Developments in Economic Geology*, Elsevier, Amsterdam 441 pp.
- Bardossy, G., Aleva, G.J.J., 1990. Lateritic Bauxites. *Developments in Economic Geology*, Elsevier, Amsterdam 624 pp.
- Bardossy, G., Combes, P.J., 1999. Karst bauxites: interfingering of deposition and palaeoweathering. In: Thiry, M., Simon-Coin on, R. (Eds.), *Palaeoweathering, Palaeosurfaces and Related Continental Deposits*. International Association of Sedimentology, Special Publications 27, Blackwell, Oxford, pp. 189–206.
- Birkeland, P.W., 1999. *Soils and Geomorphology*. Oxford University Press, New York 372pp.
- Boulang e, B., Ambrosi, J.P., Nahon, D., 1997. Laterites and bauxites. In: Paquet, H., Clauer, N. (Eds.), *Soils and Sediments. Mineralogy and Geochemistry*, Springer, Berlin, Heidelberg, pp. 49–65.
- Bown, T.M., Kraus, M.J., 1987. Integration of channel and floodplain suites; I. Developmental sequence and lateral relations of alluvial Paleosols. *J. Sediment. Res.* 57, 587–601.
- Brindley, G.W., Brown, G., 1980. *Crystal Structures of Clay Minerals and their X Ray Identification*. Mineralogical Society Monography 5. Society, London, UK, Mineralogical 495 pp.
- Budyko, M.L., Ronov, A.B., Yanshin, A.L., 1987. *History of the Earth's Atmosphere*. Springer, New York 139 pp.
- Buol, S.W., Southard, R.J., Graham, R.C., McDaniel, P.A., 2003. *Soil Genesis and Classification*. Iowa State Press, Ames, Iowa, USA 360 pp.
- Butt, C., Lintern, M.J., Anand, R.L., 2000. Evolution of regoliths and landscapes in deeply weathered terrain - Implications for geochemical exploration. *Ore Geol. Rev.* 16, 167–183.
- Chamley, H., 1989. *Clay Sedimentology*. Springer, New York 623pp.
- Chumakov, N.M., Zharkov, M.A., Herman, A.B., Doludenko, M.P., Kalandadze, N.M., Lebedev, E.L., Ponomarenko, A.G., Rautian, A.S., 1995. Climatic belts of the mid-cretaceous time. *Stratigr. Geol. Correl.* 3, 241–260.
- Combes, P.J., 1969. Recherches sur la g en ese des bauxites dans le Nord-Est de l'Espagne, le Languedoc et l'Ari ege (France). M emoires du centre d' etude et de recherches g eologiques et hydrog eologiques, Fondation CERGA, Montpellier 342 pp.
- Combes, P.J., 1973. Etude g eologique sur les conditions de mise en place d'une bauxite allochtone   substratum carbonat e: le gisement de B edarieux (H erault, France). IC SLD. BA/3 eme congr es international, Nice, pp. 89–108.
- Combes, P.J., 1984. Regards sur la g eologie des bauxites; aspects r ecents sur la g en ese de quelques gisements   substratum carbonat e. *Bull. Centres Rech. Explor. Prod. Elf-Aquitaine* 8, 251–274.
- Combes, P.J., 1990. Typologie, cadre g eodynamique et g en ese des bauxites fran aises. *Geodin. Acta* 4, 91–109.
- Combes, P.J., B ardossy, G., 1994. Typologie et contr ole g eodynamique des bauxites t ethysiennes. *Comptes rendus de l'Acad emie des sciences, S erie 2. Sci. Terre Planetes* 318, 359–366.
- Combes, P.J., Bardossy, G., 1995. Geodynamics of bauxites in the Tethyan realm. In: Nearn, A.E.M., Ricou, L.E., Vrielynck, B., Decourt, J. (Eds.), *The Tethys Ocean*. Springer, Boston, MA, pp. 347–365.
- Corentin, P., Deconinck, J.F., Pellenard, P., Am edro, F., Bruneau, L., Chenot, E., Matron, B., Huret, E., Landrein, P., 2019. Environmental and climatic controls of the clay mineralogy of Albian deposits in the Paris and Vocontian basins (France). *Cretac. Res.* https://doi.org/10.1016/j.cretres.2019.104342.
- D'Argenio, B., Mindszenty, A., 1995. Bauxites and related paleokarst: tectonic and climatic event markers at regional unconformities. *Eclogae Geol. Helv.* 88, 453–500.
- Debroas, E.-J., 1990. Le flysch noir albo-cenomanien temoin de la structuration alpine   senonienne de la Zone nord-pyr en enne en Bigorre (Hautes-Pyr enes, France). *Bull. Soc. Geol. Fr.* VI, 273–285.
- Deconinck, J.F., Chamley, H., 1995. Diversity of smectite origins in Late Cretaceous sediments: example of chalks from northern France. *Clay Miner.* 30, 365–379.
- Deconinck, J.F., Amedro, F., Fiolet-Piette, A., Juignet, P., Renard, M., 1991. Contr ole pal eog eographique de la s edimentation argileuse dans le C enomanien du Boulonnais et du Pays de Caux. *Ann. Soc. G eol. Nord* 1, 57–66.
- Demangeon, P., 1965. Sur la pr esence et la signification probable de min eraux du Massif Central dans les Bauxites de l'Isthme durancien. *C. R. Acad. Sci.* 261, 2685–2688.
- Diessel, C.F., 2012. *Coal-bearing Depositional Systems*. Springer-Verlag, Berlin-Heidelberg 721 pp.
- Dubois, P., Delfaud, J., 1989. Le Bassin du Sud-Est. In: Fran ais, A.S. (Ed.), *Dynamique et m ethodes d' etude des bassins s edimentaires*. Editions Technip, Paris, pp. 277–297.
- Duchaufour, P., 1982. *Pedology*. Allen and Unwin, London 448 pp.
- Erhart, H., 1956. La g en ese des sols en tant que ph enom ene g eologique. Masson edition. *Evolution des sciences*, Paris 90pp.
- Erhart, H., 1966. Bio-Rhexistase, biostase evolutives, heterostasie. Importance de ces notions en g eologie mini ere exogene. *C. R. hebdomadaires Seances Acad. Sci. D* 263, 1049–1051.
- Fitzpatrick, R.W., 1988. Iron compounds as indicators of pedogenic processes: examples from the southern hemisphere. In: Stucki, J.W., Goodman, B.A., Schwertmann, U. (Eds.), *Iron in Soils and Clay Minerals*. Springer Netherlands, Dordrecht, pp. 351–396.
- F ollmi, K.B., 2012. Early Cretaceous life, climate and anoxia. *Cretac. Res.* 35, 230–257.
- F ollmi, K.B., Weissert, H., Lini, A., 1993. Nonlinearities in phosphogenesis and phosphorus-carbon coupling and their implications for global change. In: Wollast, R., Mackenzie, F.T., Chou, L. (Eds.), *Interactions of C, N, P and S Biogeochemical Cycles and Global Change*. Springer, Berlin, Heidelberg, pp. 447–474.
- Fournier, F., Tassy, A., Thion, I., M unch, P., Corn e, J.-J., Borgomano, J., Leonide, P., Beslier, M.-O., Fournillon, A., Gorini, C., Guennoc, P., Oudet, J., Rabineau, M., Sage, F., Touleuc, R., 2016. Pre-Pliocene Tectonostratigraphic Framework of the Provence Continental Shelf (Eastern Gulf of Lion, SE France): *Bulletin de la Soci et e G eologique de France* 187, 187–216.
- Frakes, L.A., 1979. *Climates throughout Geologic Time*. Elsevier, Amsterdam 310pp.
- Galloway, W., 1989. Genetic Stratigraphic Sequences in Basin Analysis I: Architecture and Genesis of Flooding-Surface Bounded Depositional units. *AAPG Bull.* 73, 125–142.
- Garrels, R.M., 1983. The carbonate-silicate geochemical cycle and its effect on atmospheric carbon dioxide over the past 100 million years. *Am. J. Sci.* 283, 641–683.
- Gaucher, G., 1981. Les Facteurs de la P edogen ese. G. Lelotte, Dison, Belgique 730 pp.
- Gignoux, M., 1926. *G eologie stratigraphique*. Masson, Paris 588pp.
- Giraud, F., Reboulet, S., Deconinck, J.F., Martinez, M., Carpentier, A., Br eziat, C., 2013. The Mid-Cenomanian Event in southeastern France: evidence from palaeontological and clay mineralogical data. *Cretac. Res.* 46, 43–58.
- Hallam, A., Grose, J.A., Ruffell, A.H., 1991. Palaeoclimatic significance of changes in clay mineralogy across the Jurassic-Cretaceous boundary in England and France. *Palaeogeogr. Palaeoclimatol. Palaeoecol.* 81, 173–187.
- Hardy, R., Tucker, M., 1984. X-ray powder diffraction of sediments. In: Tucker, M. (Ed.), *Techniques in Sedimentology*. Blackwell, Oxford, pp. 191–229.
- Heimhofer, U., Adatte, T., Hochuli, P.A., Burla, S., Weissert, H., 2008. Coastal sediments from the Algarve: low-latitude climate archive for the Aptian-Albian. *Int. J. Earth Sci.* 97, 785–797.
- Husson, E., 2013. Interaction g eodynamique/karstification et mod elisation g eologique 3D des massifs carbonat es: Implication sur la distribution pr evisionnelle de la karstification. Th ese de doctorat. Universit e de Montpellier 2, Montpellier 318pp.
- Iverson, R.M., 1997. The physics of debris flows. *Rev. Geophys.* 35, 245–296.
- K ampf, N., Schwertmann, U., 1983. Goethite and hematite in a chimosequence in southern Brazil and their application in classification of kaolinitic soils. *Geoderma* 29, 27–39.
- Knaust, D., 2018. The ichnogenus *Teichichnus* Seilacher, 1955. *Earth Sci. Rev.* 177, 386–403.
- Kraus, M.J., 1999. Paleosols in clastic sedimentary rocks: their geologic applications. *Earth Sci. Rev.* 47, 41–70.
- K ubler, B., Goy-Eggenberger, D., 2001. La cristallinit e de l'illite revisit ee: Un bilan des connaissances acquises ces trente derni eres ann ees. *Clay Miner.* 36, 143–157.
- K ubler, B., Jaboyedoff, M., 2000. Illite crystallinity. *C. R. Acad. Sci. IIA Earth Planet. Sci.* 331, 75–89.
- Lagabrielle, Y., Labaume, P., Saint Blanquat, M., 2010. Mantle exhumation, crustal denudation, and gravity tectonics during Cretaceous rifting in the Pyrenean realm (SW Europe): Insights from the geological setting of the Iherzolite bodies. *Tectonics* 29, 26. <https://doi.org/10.1029/2009TC002588>.
- Larqu e, P., Weber, F., 1975. Technique de pr eparation des min eraux argileux en vue de l'analyse par diffraction des rayons X; Mise au point collective. Coll. «Note technique». Institut de G eologie, Universit e Louis-Pasteur, Strasbourg 33 pp.
- Larson, R.L., 1991. Geological consequences of superplumes. *Geology* 19, 963–966.
- L ohr, S.C., Grigorescu, M., Cox, M.E., 2013. Iron nodules in ferric soils of the Fraser Coast, Australia: relicts of laterisation or features of contemporary weathering and pedogenesis? *Soil Res.* 51, 77–93.
- Ludvigson, G.A., Joeckel, R.M., Murphy, L.R., Stockli, D.F., Gonzalez, L.A., Suarez, C.A., Kirkland, J.L., Al-Suwaidi, A., 2015. The emerging terrestrial record of Aptian-Albian global change. *Cretac. Res.* 56, 1–24.
- Lukens, W.E., Nordt, L.C., Stinchcomb, G.E., Driese, S.G., Tubbs, J.D., 2018. Reconstructing pH of paleosols using geochemical proxies. *J. Geol.* 126, 427–449.
- Mack, G.H., James, W.C., Monger, H.C., 1993. Classification of paleosols. *Geol. Soc. Am. Bull.* 105, 129–136.
- Marchand, E., 2019. R ole des interactions tectonique-s edimentation sur l' volution et la variabilit e spatiale d'un gisement de bauxite karstique: exemple du bassin de Villeveyrac (Sud de France). Universit e de Montpellier-IMT Mines Al es, Th ese de Doctorat 374 pp.
- Marchand, E., S eranne, M., Bruguier, O., Vinches, M., 2020. LA-ICP-MS dating of detrital zircon grains from the Cretaceous allochthonous bauxites of Languedoc (south of France): Provenance and geodynamic consequences. *Basin Res.* 00 (1), 1–21. <https://doi.org/10.1111/bre.12465>.
- Migon, P., 2004. *Planation surface*. In: Goudie, A.S. (Ed.), (org.). *Encyclopedia of Geomorphology*, 2 vols. Routledge, London, pp. 788–792.
- Mindszenty, A., 2010. Bauxite deposits of G ant (V ertes Hills, Hungary). *Acta Mineral. Petrogr. Field Guide Series* 11, 1–11.
- Mindszenty, A., 2016. Bauxites: feedbacks of system Earth at greenhouse times. *Geol. Croat.* 69, 79–87.
- Mongelli, G., Boni, M., Buccione, R., Sinisi, R., 2014. Geochemistry of the Apulian karst bauxites (southern Italy): chemical fractionation and parental affinities. *Ore Geol. Rev.* 63, 9–21.
- Mongelli, G., Buccione, R., Sinisi, R., 2015. Genesis of autochthonous and allochthonous Apulian karst bauxites (Southern Italy): climate constraints. *Sediment. Geol.* 325, 168–176.
- Mongelli, G., Boni, M., Oggiano, G., Mamelì, P., Sinisi, R., Buccione, R., Mondillo, N., 2017. Critical metals distribution in Tethyan karst bauxite: the cretaceous Italian ores. *Ore Geol. Rev.* 86, 526–536.
- Nahon, 1986. Evolution of iron crusts in tropical landscapes. In: Coleman, S.M., Dethier, D. P. (Eds.), *Rates of Chemical Weathering of Rocks and Minerals*. Academic Press, New York, pp. 169–187.
- Nesbitt, H.W., 1979. Mobility and fractionation of rare earth elements during weathering of a granodiorite. *Nature* 279, 206–210.

- Nesbitt, H.W., 1992. Diagenesis and metasomatism of weathering profile, with emphasis on Precambrian paleosols. In: Martini, I.P., Chesworth, W. (Eds.), *Weathering*. Elsevier Science Publishers B.V. Amsterdam, Soils and Paleosols, pp. 127–152.
- Parrish, J.T., 1998. Interpreting Pre-Quaternary Climate from the Geologic Record. *Paleobiology and Earth History Series*. Columbia University Press, New York 338 pp.
- Pédro, G., 1984. La genèse des argiles pédologiques. Ses implications minéralogiques, physico-chimiques et hydriques/Clay genesis in pedological conditions. Mineralogical, physico-chemical and hydric implications. *Sci. Géol. Bull. Mém.* 37, 333–347.
- Peyaud, Barbarand, Carter, Pagel, 2005. Mid-Cretaceous uplift and erosion on the northern margin of the Ligurian Tethys deduced from thermal history reconstruction. *Int. J. Earth Sci.* 93, 462–474.
- Pierson, T.C., 1980. Erosion and deposition by debris flows at Mt Thomas, north Canterbury, New Zealand. *Earth Surf. Process.* 5, 227–247.
- Pracejus, B., 2008. *The Ore Minerals under the Microscope: An Optical Guide*. Atlases in geosciences, Berlin, Elsevier 875 p.
- Ramanaidou, E.R., 2009. Genesis of lateritic iron ore from banded iron-formation in the Capanema mine (Minas Gerais, Brazil). *Aust. J. Earth Sci.* 56, 605–620.
- Retallack, G.J., 1988. Field recognition of paleosols. In: Reinhart, J., Sigleo, W.R. (Eds.), *Paleosols and Weathering through Geologic Time: Principles and Application*. Geological Society of America Special Paper 216, pp. 1–20.
- Retallack, G.J., 1994. The environmental factor approach to the interpretation of paleosols. In: Amundson, R.R., Harden, J., Singer, M. (Eds.), *Factors of soil formation: A fiftieth anniversary retrospective*. 33. Soil Science Society of America, Madison, pp. 31–64.
- Retallack, G.J., 2010. Lateritization and bauxitization events. *Econ. Geol.* 105, 655–667.
- Reynolds, A.D., 1996. Paralic successions. In: Emery, D., Myer, K.J. (Eds.), *Sequence stratigraphy*. Blackwell Science, Oxford, pp. 134–177.
- Righi, D., Meunier, A., 1995. Origin of clays by rock weathering and soil formation. In: Velde, B. (Ed.), *Origin and Mineralogy of Clays*. Springer, Heidelberg, Berlin, pp. 43–161.
- Royer, D.L., 1999. Depth to pedogenic carbonate horizon as a paleoprecipitation indicator? *Geology* 27, 1123–1126.
- Ruffell, A., Worden, R., 2000. Palaeoclimate analysis using spectral gamma-ray data from the Aptian (Cretaceous) of southern England and southern France. *Palaeogeogr. Palaeoclimatol. Palaeoecol.* 155, 265–283.
- Ruffell, A., McKinley, J.M., Worden, R.H., 2002. Comparison of clay mineral stratigraphy to other proxy palaeoclimate indicators in the Mesozoic of NW Europe. *Philosophical transactions of the Royal Society of London. Series A: Mathematical. Phys. Eng. Sci.* 360, 675–693.
- Schaetzl, R., Thompson, M.L., 2005. Soil genesis and profile differentiation. In: Schaetzl, R., Anderson, S. (Eds.), *Soils-Genesis and Geomorphology*. Cambridge University Press Cambridge, UK, pp. 347–362.
- Scheepers, R., Rozendaal, A., 1993. Redistribution and fractionation of U, Th and rare-earth elements during weathering of subalkaline granites in SW Cape Province, South Africa. *J. Afr. Earth Sci.* 17, 41–50 (and the Middle East).
- Scheinost, A.C., Schwertmann, U., 1999. Color identification of iron oxides and hydroxysulfates: use and limitations. *Soil Sci. Soc. Am. J.* 63, 1463–1471.
- Schwertmann, U., 1988. Occurrence and formation of iron oxides in various pedoenvironments. In: Stucki, W., Goodmann, B.A., Schwertmann, U. (Eds.), *Iron in Soils and Clay Minerals*. Springer, Dordrecht, pp. 267–308.
- Séranne, M., Camus, H., Lucazeau, F., Barbarand, J., Quinif, Y., 2002. Surrection et érosion polyphasées de la bordure cévenole. Un exemple de morphogenèse lente. *Bull. Soc. Géol. Fr.* 173, 97–112.
- Sheldon, N.D., Tabor, N.J., 2009. Quantitative paleoenvironmental and paleoclimatic reconstruction using paleosols. *Earth Sci. Rev.* 95, 1–52.
- Spry, P.G., Gedlinske, B.L., 1987. *Economic Geology: Tables of Determination of Common Opaque Minerals*. Economic Geology Publishing Company, New Haven 52 pp.
- Srivastava, P., Bhattacharyya, T., Pal, D.K., 2002. Significance of the formation of calcium carbonate minerals in the pedogenesis and management of cracking clay soils (Vertisols) of India. *Clay Clay Miner.* 50, 111–126.
- Środoń, J., 2009. Quantification of illite and smectite and their layer charges in sandstones and shales from shallow burial depth. *Clay Miner.* 44, 421–434.
- Stein, M., Arnaud-Vanneau, A., Adatte, T., Fleitmann, D., Spangenberg, J.E., Foellmi, K.B., 2012. Palaeoenvironmental and palaeoecological change on the northern Tethyan carbonate platform during the Late Barremian to earliest Aptian. *Sedimentology* 59, 939–963.
- Suarez, M.B., González, L.A., Ludvigson, G.A., 2011. Quantification of a greenhouse hydrologic cycle from equatorial to polar latitudes: the mid-Cretaceous water bearer revisited. *Palaeogeogr. Palaeoclimatol. Palaeoecol.* 307, 301–312.
- Tavani, S., Bertok, C., Granado, P., Piana, F., Salas, R., Vigna, B., Munoz, J.A., 2018. The Iberia-Eurasia Plate Boundary East of the Pyrenees: Earth-Science Reviews 187, 314–337.
- Thiry, M., 2000. Palaeoclimatic interpretation of clay minerals in marine deposits: an outlook from the continental origin. *Earth Sci. Rev.* 49, 201–221.
- Thornthwaite, C.W., 1948. An approach toward a rational classification of climate. *Geogr. Rev.* 38, 55–94.
- Valeton, I., 1972. *Bauxites*. Elsevier, Amsterdam 226 pp.
- Valeton, I., Biermann, M., Reche, R., Rosenberg, F., 1987. Genesis of nickel laterites and bauxites in Greece during the Jurassic and Cretaceous, and their relation to ultrabasic parent rocks. *Ore Geol. Rev.* 2, 359–404.
- Vallance, J.W., Scott, K.M., 1997. The Osceola Mudflow from Mount Rainier: sedimentology and hazard implications of a huge clay-rich debris flow. *Geol. Soc. Am. Bull.* 109, 143–163.
- Weaver, C.E., 1989. *Clays, Muds, and Shales*. Elsevier, New York 819 pp.
- Wright, V.P., 1992. Paleosol recognition: a guide to early diagenesis in terrestrial settings. In: Wolf, K.H., Chilingarian, G.V. (Eds.), *Diagenesis. III*. Elsevier, Amsterdam, pp. 591–619.
- Wyns, R., Quesnel, F., Simon-Coincon, R., Guillocheau, F., Lacquement, F., 2003. Major weathering in France related to lithospheric deformation. *Géol. Fr.* 1, 79–87.